A LABORATORY STUDY OF DYNAMIC LOAD-DEFORMATION AND DAMPING PROPERTIES OF SANDS CONCERNED WITH A PILE-SOIL SYSTEM

by

Paul C. Chan
Research Assistant

T. J. Hirsch
Associate Research Engineer

and

Harry M. Coyle
Assistant Research Engineer

Research Report Number 33-7

Piling Behavior Research
Research Study Number 2-5-62-33

Sponsored by
The Texas Highway Department

In cooperation with the
U. S. Department of Transportation, Federal Highway Administration
Bureau of Public Roads

June, 1967

TEXAS TRANSPORTATION INSTITUTE
Texas A&M University
College Station, Texas

PREFACE

The information contained herein was developed on Research Study 2-5-62-33 entitled "Piling Behavior" which is a cooperative research study sponsored jointly by the Texas Highway Department and the U. S. Department of Transportation, Bureau of Public Roads. The broad objective of this project is to fully develop the use of the computer solution of the wave equation so that it may be used to predict driving stresses in piling and be used to estimate static load bearing capacity of piling from driving resistance records.

This report concerns itself with the specific objective of determining the dynamic load-deformation properties of soils. These properties are necessary for the wave equation analysis and have been found to have a significant effect on the driving stresses and pile penetration during driving. Only one of the six previous reports on this study has dealt with the Soil Mechanics aspects of this research. This report was No. 33-5 entitled "An Annotated Bibliography—Soil Dynamics and Soil Rheology," and was published in June, 1966. The other five previous reports all dealt with the structural aspects of the piling behavior problem.

This report should be considered as an interim report of exploratory investigations into the dynamic load-deformation properties of sands. A considerable amount of time was spent on developing instrumentation alone, and this report describes this instrumentation. In addition, this report presents preliminary test results on the dynamic properties of Ottawa and Victoria sands. The study of the dynamic load-deformation properties of sands is being continued in the 1966-67 year. In addition, work on the dynamic properties of clays was started during the 1966-67 year. To the knowledge of the authors, dynamic tests on saturated sand samples at the higher loading velocities used in this study have never been conducted in the past.

The opinions, findings and conclusions expressed in this report are those of the authors and not necessarily those of the Bureau of Public Roads.

TABLE OF CONTENTS

LIST OF TABLES

LIST OF FIGURES

A Laboratory Study of Dynamic Load-Deformation and Damping Properties of Sands Concerned with A Pile-Soil System

Chapter I

INTRODUCTION

1.1. Purpose and Scope

Foundation piles of many kinds have been used for centuries and the driving and design of a satisfactory pile foundation is often dependent upon experience and judgement. For well over 100 years, engineers have attempted to derive dynamic pile driving formulas which would serve to establish the static bearing capacity of piles. However, many engineers today realize that the numerous dynamic pile driving formulas which have been used, and are still being used, have serious limitations and cannot be depended upon to give reliable results. But they are still used for lack of an adequate substitute. The possibility of relating the behavior of a pile during driving to its static load carrying capacity by the use of the wave equation method of pile driving analysis is encouraging.

This method is based on the theory of longitudinal stress wave transmission that is covered in a general way by the wave equation. Furthermore, it also considers influencing factors such as the use of capblocks, pile caps, cushion blocks, composite piles, as well as shear characteristics of soils under dynamic loading. As a result, the wave equation method is not just another dynamic pile driving formula, but rather, it is an analytical method which is well founded.

A systematic investigation of applying the wave equation concept on pile driving has been performed by the staff of the Structural Research Department of the Texas Transportation Institute. The papers published thus far on this subject matter may be divided into two main phases. The first is concerned with programming of the computer solution of the wave equation (Refs. 14, 23, and 24) and theoretical stress analysis (Ref. 16). The second phase is concerned with field measurements (Ref. 15) and experimental investigations (Ref. 13). This study is an exploratory study concerning the second phase.

1.2 Wave Equation Application to Pile Driving

Historically, the problem of longitudinal impact of elastic bars was discussed by Cauchy, Poisson, and finally by Saint-Venant in 1866, and the final solution was given by J. Boussinesq in 1883 (Ref. 34). It can be shown that the differential equation of one-dimensional propagation of stress waves is of the form:

$$\frac{\partial^2 D}{\partial t^2} = c^2 \frac{\partial^2 D}{\partial x^2} \qquad (1\text{-}1)$$

where D is the displacement of a point x along the bar, t is the time, and c is the velocity of propagation of the disturbance which is found to be related to the modulus of elasticity, E, and the density, ρ, of the material in the following way:

$$c^2 = \frac{E}{\rho} \qquad (1\text{-}2)$$

In 1931, Issacs (Ref. 18) pointed out the occurrence of the wave action in pile driving. Following Issac's proposal, Glanville, Grime, and Davis in 1935 (Ref. 11) and Glanville, Grime, Fox, and Davis in 1938 (Ref. 12) published the results of extensive mathematical and experimental studies of piling in which wave propagation was considered.

Pertaining to the above work, Cummings (Ref. 8) commented as follows:

> "Pile driving is far more closely related to the St. Venant-Boussinesq theory of longitudinal impact rods than it is to Newtonian theory of the impact of spheres.
>
> "The fact that the theory of longitudinal impact leads to this conclusion is of considerable practical importance. Nevertheless, there can be no question about the validity of applying the theory of longitudinal impact to pile driving.
>
> "From this comparison, it seems reasonably evident that the stress transmission characteristics of a pile are often far more important than its inertia."

Unfortunately, electronic computers were not available at that time making possible the solution of such complex problems. Consequently, the application of wave equation in this problem necessarily involved simplifying assumptions.

In 1955, Smith (Ref. 27) proposed a method of treating one-dimensional longitudinal impact for approximate solution of elastic bar problems. He replaced the actual bars by a model consisting of a number of discrete masses and springs of suitable dimensions. For these, he set up the equations of motion in the form of a set of finite difference equations which can be solved by numerical iteration with slide rule, desk calculator or electronic digital calculator. Smith extended the method to general problems of complex character such as those including variable resistance (damping friction) and plastic flow. As a result, this led to the solution of this complex pile driving problem. The Smith mathematical model for driving-equipment-pile-soil system is as shown in Fig. 1-1. For a detailed discussion of the development of the mathematical model, the reader is referred to the original work of Smith (Ref. 28). The

following description has been given by Samson, et al. (Ref. 24).

Fig. 1-1 illustrates the idealization of the pile system suggested by Smith. In general, the system is considered to be composed of (see Fig. 1-1a):

1. A ram, to which an initial velocity is imparted by the pile driver;
2. A capblock (cushioning material);
3. A pile cap;
4. A cushion block (cushioning material);
5. A pile; and
6. The supporting medium, or soil.

In Fig. 1-1 are shown the idealizations for the various components of the actual pile. The ram, capblock, pile cap, cushion block, and pile are pictured as appropriate discrete weights and springs. The frictional soil resistance on the side of the pile is represented by a series of side springs; the point resistance is accounted for by a single spring at the point of the pile. The characteristics of these various components will be discussed in greater detail.

Actual situations may deviate from that in Fig. 1-1. For example, a cushion block may not be used or an anvil may be placed between the ram and capblock. Such cases are readily accommodated.

Internal Springs. The ram, capblock, pile cap, and cushion block may in general be considered to consist

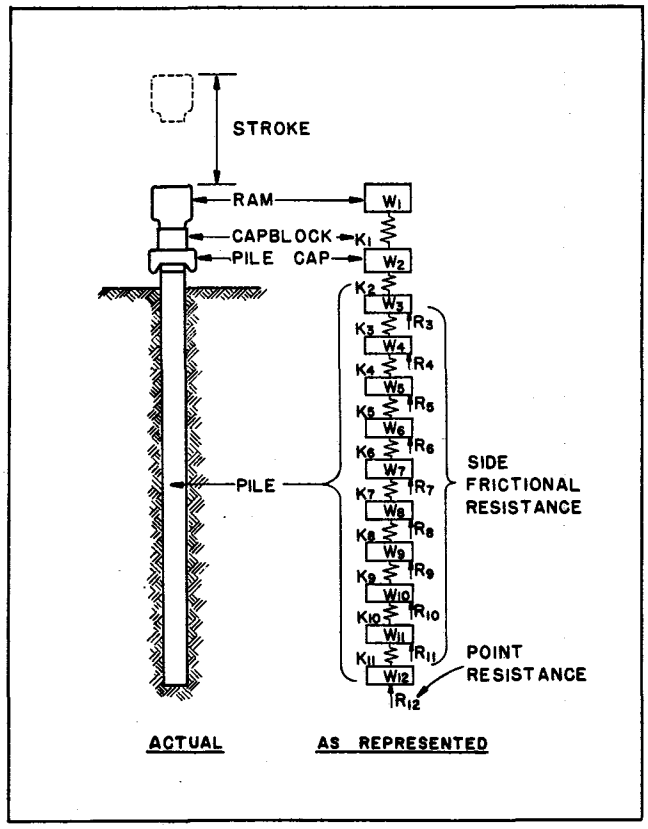

Figure 1-1. Method of representing pile for purpose of calculation (after Smith, Ref. 24).

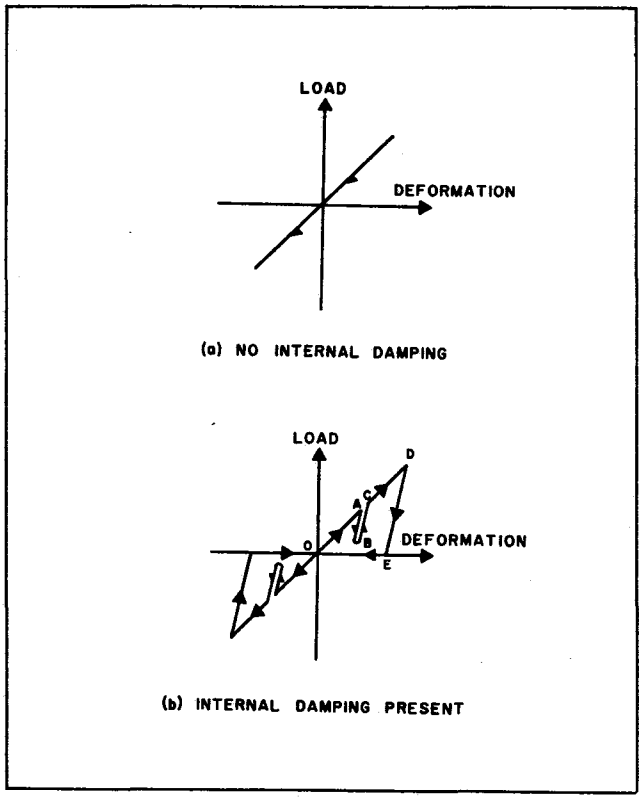

Figure 1-2. Load-deformation relationships for internal springs.

of "internal" springs, although in the representation of Fig. 1-1b the ram and the pile cap are treated as though rigid (a reasonable assumption for many practical cases).

Figs. 1-2a and 2b suggest different possibilities for representing the load-deformation characteristics of the internal springs. In Fig. 1-2a, the material is considered to experience no internal damping. In Fig. 1-2b, the material is assumed to have internal damping according to the linear relationship shown.

External Springs. The resistance to dynamic loading afforded by the soil in shear along the outer surface of the pile and in bearing at the point of the pile is not clearly understood. Fig. 1-3 shows the load-deformation characteristics assumed for the soil in Smith's procedure, exclusive of damping effects. The path OABCDEFG represents loading and unloading in side friction. For the point, only compressive loading may take place and the loading and unloading path would be along OABCF.

It is seen that the characteristics of Fig. 1-3 are defined essentially by the quantities "Q" and "Ru." "Q" is termed the quake and represents the maximum deformation which may occur elastically. "Ru" is the ultimate ground resistance, or the load at which a spring behaves purely plastically.

A load-deformation diagram of the sort of Fig. 1-3 may be established separately for each spring. Thus, K'(m) equals Ru(m) divided by Q(m), where K'(m) is the spring constant (during elastic deformation) for external spring m.

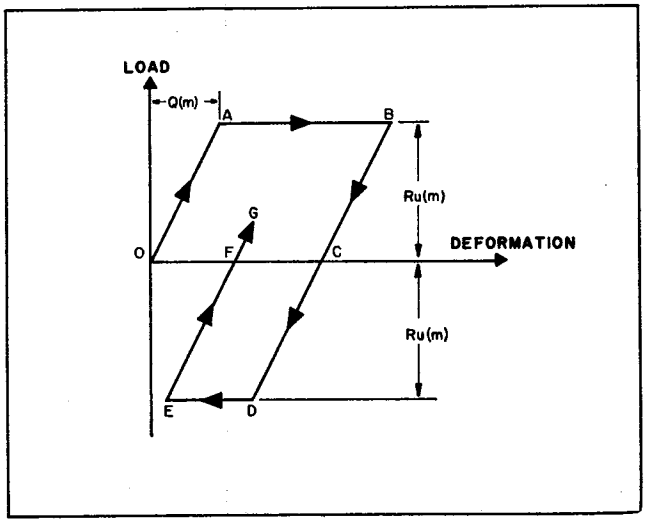

Figure 1-3. Load-deformation characteristics assumed for soil spring m.

Basic Equations. Equations (1-3) through (1-7) are developed by Smith (Ref. 28).

$$D(m,t) = D(m,t-1) + 12\Delta t\ V(m,t-1) \quad (1\text{-}3)$$

$$C(m,t) = D(m,t) - D(m+1,t) \quad (1\text{-}4)$$

$$F(m,t) = C(m,t)\ K(m) \quad (1\text{-}5)$$

$$R(m,t) = [D(m,t) - D'(m,t)]\ K'(m)\ [1 + J(m)V(m,t-1)] \quad (1\text{-}6)$$

$$V(m,t) = V(m,t-1) + [F(m-1,t) - F(m,t) - R(m,t)]\ \frac{g\Delta t}{W(m)} \quad (1\text{-}7)$$

where

( ) = functional designation;

m = element number;

t = number of time interval;

Δt = size of time interval (sec.);

C(m,t) = compression of internal spring m in time interval t (in.);

D(m,t) = displacement of element m in time interval t (in.);

D'(m,t) = plastic displacement of external spring m in time interval t (in.);

F(m,t) = force in internal spring m in time interval t (lb.);

g = acceleration due to gravity (ft. per sec.^{2});

J(m) = damping constant of soil at element m (sec. per ft.);

K(m) = spring constant associated with internal spring m (lb. per in.);

K'(m) = spring constant associated with external spring m (lb. per in.);

R(m,t) = force exerted by external spring m on element m in time interval t (lb.);

V(m,t) = velocity of element m in time interval t (ft. per sec.); and

W(m) = weight of element m (lb.).

This notation which differs slightly from that used by Smith (Ref. 28) was suggested by Samson, et al. (Ref. 24). Also, Smith restricts the soil damping constant J to two values, one for the point of the pile in bearing and one for the side of the pile in friction. While the present knowledge of damping behavior of soils perhaps does not justify greater refinement, it is reasonable to follow Samson's notation as a function of m for the sake of generality.

The use of a spring constant K(m) implies a load-deformation behavior of the sort shown in Fig. 1-2a. For this situation, K(m) is the slope of the straight line. Smith develops special relationships to account for internal damping in the capblock and the cushion block. He obtains instead of Eq. 1-5 the following equation:

$$F(m,t) = \frac{K(m)}{[e(m)]^2}\ C(m,t) - \left\{ \frac{1}{[e(m)]^2} - 1 \right\} K(m)\ C(m,t)_{max} \quad (1\text{-}8)$$

where

e(m) = coefficient of restitution of internal spring m; and

$C(m,t)_{max}$ = temporary maximum value of C(m,t).

With reference to Fig. 1-1, Eq. (1-8) would be applicable in the calculation of the forces in internal springs m = 1 and m = 2. The load-deformation relationship characterized by Eq. (1-8) is illustrated by the path OABCDEO in Fig. 1-2b. For a pile cap or a cushion block, no tensile forces can exist; consequently, only this part of the diagram applies. Intermittent unloading-loading is typified by the path ABC, established by control of the quantity $C(m,t)_{max}$ in Eq. (1-8). The slopes of lines AB, BC, and DE depend upon the coefficient of restitution e(m).

The computations proceed as follows:

1. The initial velocity of the ram is determined from the properties of the pile driver. Other time-dependent quantities are initialized at zero.

2. Displacements D(m,1) are calculated by Eq. (1-3). It is to be noted that V(1,0) is the initial velocity of the ram.

3. Compressions C(m,1) are calculated by Eq. (1-4).

4. Internal spring forces F(m,1) are calculated by Eq. (1-5) or Eq. (1-8) as appropriate.

5. External spring forces R(m,1) are calculated by Eq. (1-6).

6. Velocities V(m,1) are calculated by Eq. (1-7).

7. The cycle is repeated for successive time intervals.

In Eq. (1-6), the plastic deformation D'(m,t) for a given external spring follows Fig. (1-3) and may be determined by special routines. For example, when D(m,t) is less than Q(m), D'(m,t) is zero; when D(m,t) is greater than Q(m) along line AB (see Fig. 3), D'(m,t) is equal to D(m,t) − Q(m).

Smith notes that Eq. (1-6) produces no damping when D(m,t) − D'(m,t) becomes zero. He suggests an

alternate equation to be used after D(m,t) first becomes equal to Q(m):

$$R(m,t) = [D(m,t) - D'(m,t)]\ K'(m) + J(m)\ K'(m)\ Q(m)\ V(m,t-1) \quad (1\text{-}9)$$

Care must be used to satisfy conditions at the head and point of the pile. Consider Eq. (1-5). When m = p, where p is number of the last element of the pile, K(p) must be set equal to zero since there is no F(p,t) force (see Fig. 1-1). Also, at the point of the pile, the soil spring must be prevented from exerting tension on the pile point. In applying Eq. (1-7) to the ram (m = 1), one should set F(0,t) equal to zero.

For the idealization of Fig. 1-1, it is apparent that the spring associated with K(2) represents both the cushion block and the top element of the pile. It may be obtained by the following equation:

$$\frac{1}{K(2)} = \frac{1}{K(2)_{\text{cushion}}} + \frac{1}{K(2)_{\text{pile}}} \quad (1\text{-}10)$$

A more complete discussion of digital-computer programming details and recommended values for various physical quantities are given in (Ref. 28).

From the point of view of basic mechanics, the wave equation method is a method of analysis which is well founded physically and mathematically. An excellent explanation of various pile driving conditions has been given by Hirsch (Ref. 16).

1.3. The Present Status of the Problem

Review of the literature on dynamic load-deformation characteristics of cohesionless soils has been published separately (Ref. 5). However, the limited past investigations on the subject matter were performed for a specific purpose. As a result, the application of wave equation in pile driving analysis has been hampered by the lack of comprehensive and reliable data on the fundamental properties of soils subjected to very rapidly applied load. The present status of the problem can be well understood as Smith pointed out in the conclusion of his paper (Ref. 28).

> "The knowledge of soil mechanics is incomplete, especially the knowledge of soil mechanics under pile driving action. This offers a fertile field for future investigation, especially now that a mathematical method of calculating driving action is available for checking and analyzing field test results."

It was also correctly observed by Hirsch (Ref. 15):

> ". . . Up to the present time no experiments have been performed to determine accurately the last two constants, damping, and 'quake' . . . ."

1.4. Objective and Outline of the Study

The principal objective of the investigation which is described in this paper was to provide the needed information concerning the load-deformation properties of sands under rapidly applied loads similar to those found at the point of a pile in a pile-soil system.

An attempt has been made to achieve the objective of the study through the following main steps:

1. To develop an apparatus to measure load-deformation of a cohesionless soil under a rapidly applied load.

2. To evaluate the dynamic behavior of cylindrical specimens of a cohesionless soil subjected to various rates of loading.

3. To investigate the feasibility of a rheological model to simulate the dynamic load characteristics of a cohesionless soil under rapidly applied loads.

Chapter II

MECHANICS OF TRIAXIAL COMPRESSION TEST ON COHESIONLESS SOILS

Research data concerning the mechanical behavior of cohesionless soil under a dynamic load is very limited. However, much study has been devoted to the ultimate strength of soils under static load, and much has been written on this subject by various writers (Refs. 3, 30, 31 and 32). This chapter will review some of the basic principles which were used to formulate the test program given in later chapters.

2.1. The Triaxial Test

A detailed account of the triaxial test has been presented by Bishop and Henkel (Ref. 2) in a recent nomograph. The essentials of the device are indicated in Fig. 2-1. The soil cylinder is normally 1.4 to 3.0 in. in diameter with a length roughly 2.0 to 2.5 times the diameter. The pressure cell usually consists of a lucite cylinder with rigid metal pedestals. Either gas or fluid is used within the cell to apply confining pressure. Force is applied to the loading piston either by dead weight, or by geared or hydraulic loading presses. The axial force and the change in length of the specimen are measured; in addition, the pressure within the pore phase of the soil is sometimes measured.

If a laboratory test is to indicate the behavior of soil within an actual soil deposit, it is necessary to simulate as closely as possible the field conditions, such as drainage control, density, lateral confining pressure, loading rates, etc. Considerable judgment and experience are still necessary in this aspect of triaxial testing. Discussions were outlined by Professor S. J. Buchanan (Ref. 3) in an advanced Soil Mechanics course at Texas A&M University.

In general, triaxial tests are classified according to the conditions of drainage during different stages of load application.

1. Undrained Tests—The standard undrained test is a compression test performed under constant lateral

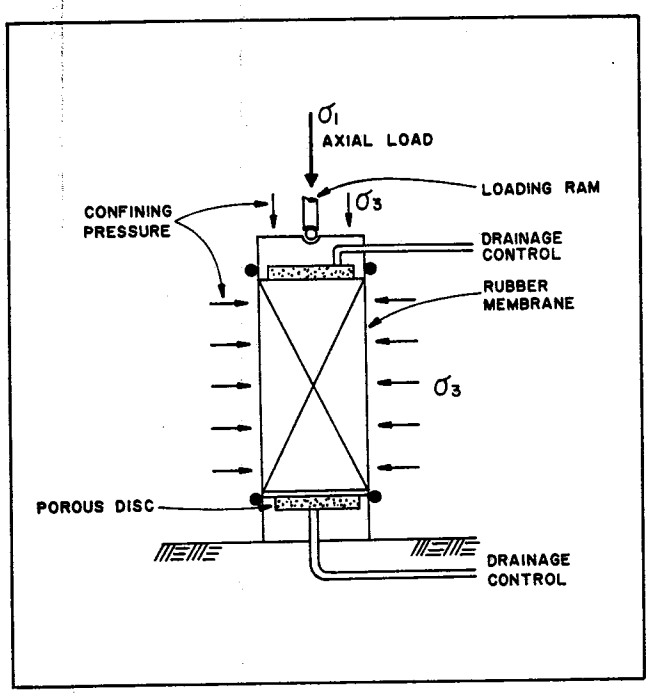

Figure 2-1. Schematic of triaxial compression test.

confining pressure. This means that the minor principal stress, σ_3, is maintained at a constant value while failure results from the increase in the major principal stress, σ_1 (see Fig. 2.1).

2. Consolidated-Undrained Tests — Drainage is permitted during the application of lateral confining pressure, σ_3, so that the soil specimen is fully consolidated under this pressure. No drainage is allowed during the application of the major principal stress, σ_1.

3. Drained Tests—Drainage is allowed throughout the test so that no excess pore pressure is set up during the application of the major principal stress, σ_1.

2.2. The Coulomb-Hvorslev Failure Criterion

A discussion of the shear strength of soils is found in an essay written by Coulomb (Ref. 7) published in 1773, and entitled "Essai sur une application des regles de Maximis et Minimis a quel ques Problemes de Statique, relatifs a l'Architecture." Coulomb introduced the first failure criterion for soil, assuming that resistance to failure is regarded as essentially friction in nature. The shear stress, τ, causing slip on any plane is taken as the sum of a constant value, termed the cohesion, and an additional amount that is proportional to the normal pressure acting across the plane. Thus,

$$\tau = c + \sigma \tan \phi \qquad (2\text{-}1)$$

in which c is the cohesion, σ denotes the normal stress across the plane, and ϕ is the angle of internal friction of the material. This equation is relatively simple, but the values of c and ϕ depend on many factors and may vary between wide limits.

A modified form of Eq. (2-1) was suggested by Hvorslev (Ref. 16) by expressing the shear strength as a function of the effective normal stress, $\bar{\sigma}$, in accordance with Terzaghi's fundamental concept that the strength and deformation characteristics of soils are governed by the *effective stress* rather than the total stresses. Thus, one can rewrite Eq. (2-1) in the following form:

$$\tau = c + \bar{\sigma} \tan \phi \qquad (2\text{-}2)$$

For cohesionless soils, Eq. (2-2) may be expressed as

$$\tau = \bar{\sigma} \tan \phi$$

or

$$\tau = (\sigma - \mu) \tan \phi \qquad (2\text{-}3)$$

where μ is the pore pressure, and σ is the total pressure.

It is most important to maintain the above established definitions of Eq. (2-3), which is called the effective stress concept.

On the basis of Eq. (2-3), Skempton (Ref. 26) proposed a more rigorous analysis as given in the following paragraphs. Let us consider the forces acting across a surface in a granular soil as shown in Fig. 2-2 which approximates a plane passing through the pore space and points of contact of the soil particles. Fig. 2-2 is, of course, a qualitative representation for a typical cross section through two grains in contact. For the purpose of this discussion, molecular forces, if any, are not taken into account. The normal stress is then equal to the average force per unit area perpendicular to this plane, and areas are considered as projected onto the plane.

Let P denote the total load

A = the gross area

A_s = the area of contact between grains

A_w, A_g = the areas of contact between water and soil and air and soil, respectively

p_s, p_w, and p_g = the stresses in solid, liquid and gaseous, respectively

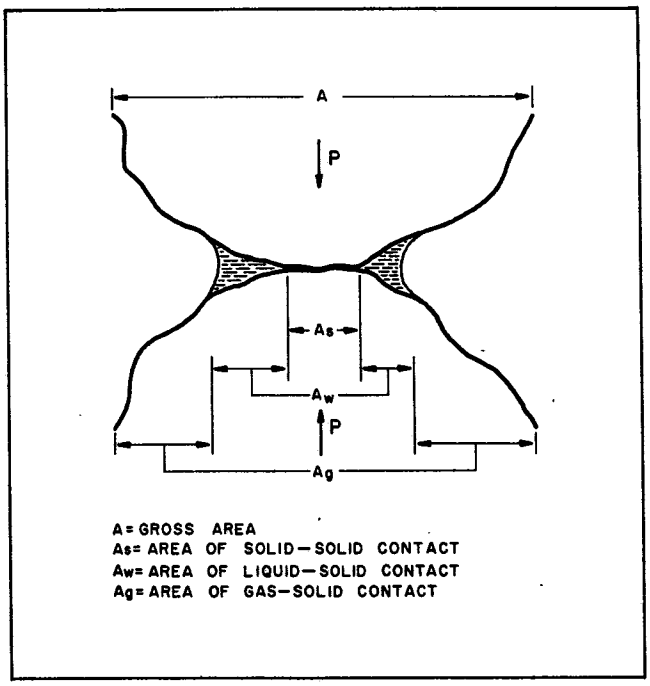

Figure 2-2. Effective stress on area.

Considering in this instance the balance of forces over the cross-sectional area only, we see that

$$P = p_s A_s + p_w A_w + p_g A_g \qquad (2\text{-}4)$$

or dividing both sides by the gross area A, we find that

$$\frac{P}{A} = \frac{A_s}{A} p_s + \frac{A_w}{A} p_w + \frac{A_g}{A} p_g$$

or

$$\sigma = \alpha p_s + \chi p_w + (1 - \alpha - \chi) p_g \qquad (2\text{-}5)$$

where σ is the total stress over the gross area, and α, χ and $(1 - \alpha - \chi)$ are the ratios of areas of solid, liquid, and gaseous, respectively, in contact with the solid, to the gross area A. The parameter is related to the degree of saturation of the soil.

Alternatively, Eq. (2-5) may be put in the form

$$\sigma = \alpha p_s + (1-\alpha) p_w + (1-\alpha-\chi)(p_g - p_w) \qquad (2\text{-}6)$$

in which the terms in parentheses represent equivalent pore pressures due to the pressure in the liquid and gaseous phases. If the soil is completely saturated, then $(1 - \alpha - \chi) = 0$, and Eq. (2-6) becomes

$$\sigma = \alpha p_s + (1 - \alpha) p_w \qquad (2\text{-}7)$$

The ratio, α, the area of actual solid contact to total area, will be very small. Careful estimates (Ref. 1) show that it cannot be greater than a few hundredths of the cross-sectional area of soil. Hence, the term $(1-\alpha)$ approaches unity. However, the stress in the solids part of the interface is very high, the product p_s does not become equal to zero but to a quantity which is called the effective stress in the soil skeleton. Consequently,

$$\sigma = \overline{\sigma} + p_w$$

or

$$\overline{\sigma} = \sigma - \mu \qquad (2\text{-}8)$$

in which $p_w = \mu$. The effective stress concept may be said to be semiempirical, but its practical validity has been demonstrated in many laboratory tests and field observations.

2.3. *Mohr's Shear Strength Diagram*

Following the earlier work of Coulomb, Mohr developed his famous stress circle. The Mohr's stress circle is a method which allows a graphical determination of the stresses on different planes through a point of a stressed body. The abscissas of the Mohr's circle represent the normal stresses on a plane, and ordinates to the stress circle give the shear stresses on different planes through the considered point. The diameter of the stress circle is equal to the difference between the major and minor principal stresses. Mathematically, this provides a functional relationship between the normal stress, σ, and shear stress, τ, on the failure plane, i. e.,

$$\tau = f(\sigma) \qquad (2\text{-}9)$$

Since the theory involves two parameters, i. e., σ and τ, the curve defined by this functional relationship may be plotted on a plane as shown in Fig. 2.3. The line OA is termed the Mohr rupture envelope which represents the locus of all points defining the limiting values of both components of σ and τ on the slip planes

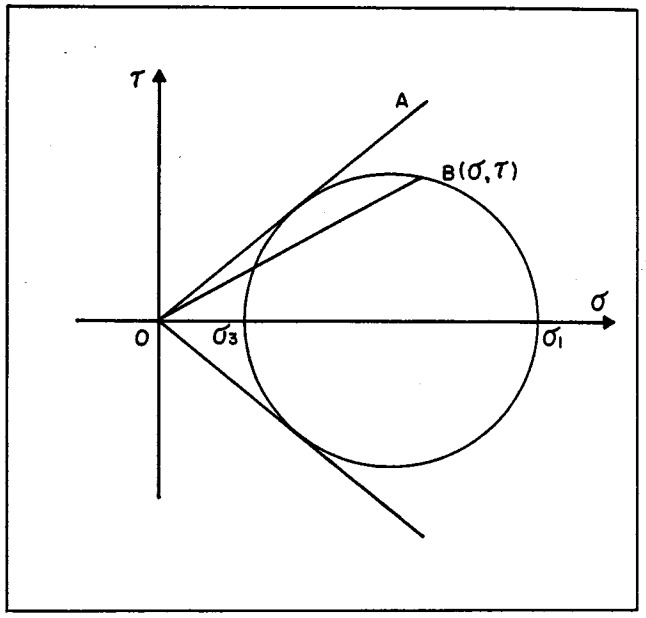

Figure 2-3. Two dimensional Mohr's circle.

under the stress system to which the material may be subjected. The theory is attractive for use in studying the shear strength of soils since there is no requirement that the material follow Hooke's law or that Poisson's ratio be constant. Moreover, the strength and stiffness of the material in tension and compression need not be equal.

As an example, in Fig. 2-4, a Mohr diagram is shown. The shear stress τ, and the normal stress σ

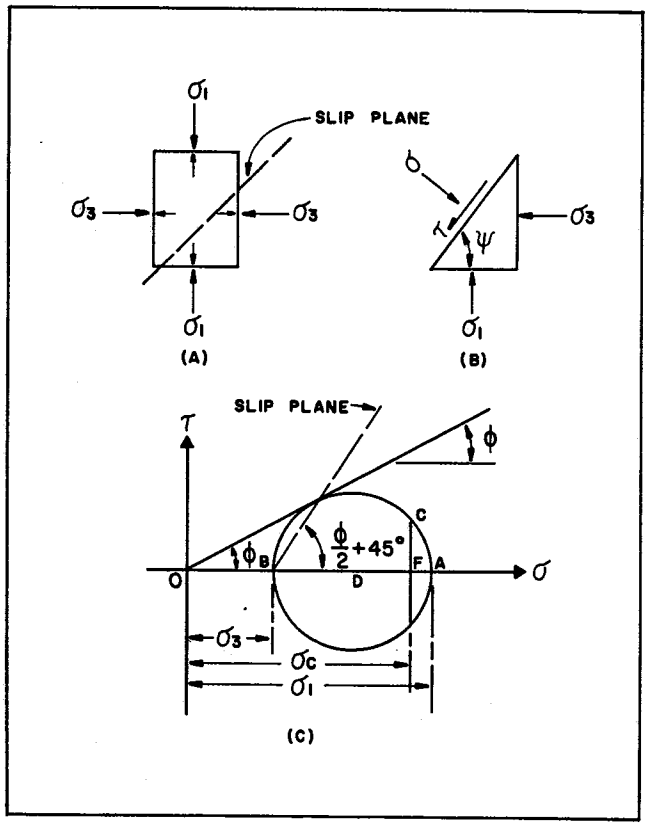

Figure 2-4. Mohr's circle diagram of stresses.

acting on the plane which is at an angle Ψ to the major principal stress can be determined. Thus, the analytical expressions for these stresses are (Ref. 30):

$$\sigma = \sigma_1 \sin^2 \Psi + \sigma_3 \cos^2 \Psi \qquad (2\text{-}10)$$

$$\tau = \tfrac{1}{2} (\sigma_1 - \sigma_3) \sin 2\Psi \qquad (2\text{-}11)$$

Furthermore, a Mohr failure envelope is a graphical representation of the limiting shear strength on different planes through a point of a soil mass, and gives the strength as a function of the normal stresses on these planes.

For cohesionless material, the failure line is represented by the equation: (See Eq. 2-3.)

$$\tau = (\sigma - \mu) \tan \phi$$

For a triaxial compression test of cohesionless material, Eq. (2-3) leads to the following expression for maximum axial stress:

$$\sigma_1 = \frac{1 + \sin \phi}{1 - \sin \phi} \sigma_3$$

or

$$\sigma_1 = \sigma_3 \tan^2 \left(45° + \frac{\phi}{2} \right) \qquad (2\text{-}12)$$

A slip plane which subtends an angle of $\left(45° + \frac{\phi}{2} \right)$ to the major principal plane, is a failure plane. In this case, the failure line is valid for all planes through all points of the considered sand, provided the density is uniform.

2.4. *Physical Components of Cohesionless Soils*

The following is an attempt to give an explanation of the nature of shear strength components of a cohesionless soil and must therefore be considered qualitative and hypothetical. The material presented and discussed in the following section is mostly a summary of work done by others (Refs. 3, 30 and 33).

2.4.1. Internal Friction. Friction is intimately involved in the movement of one particle relative to another. The physical components governing development of shear strength in cohesionless soils arise from the internal friction. The components giving rise to motion include both movement by sliding and movement from interlocking action between particles. Sliding friction results from one particle moving on the other. There is a microscopic volume change associated with this action. Interlocking friction consists of the physical restraint to relative particle translation afforded by adjacent particles. Since there is particle obstruction relative to particle translation, individual particles must ride over their neighbors to provide translation. Hence, a volume increase is generally associated with the occurrence of interlocking. This action is measured by either a direct shear or triaxial test which develops both types of friction. They are not easily separable in a granular soil mass.

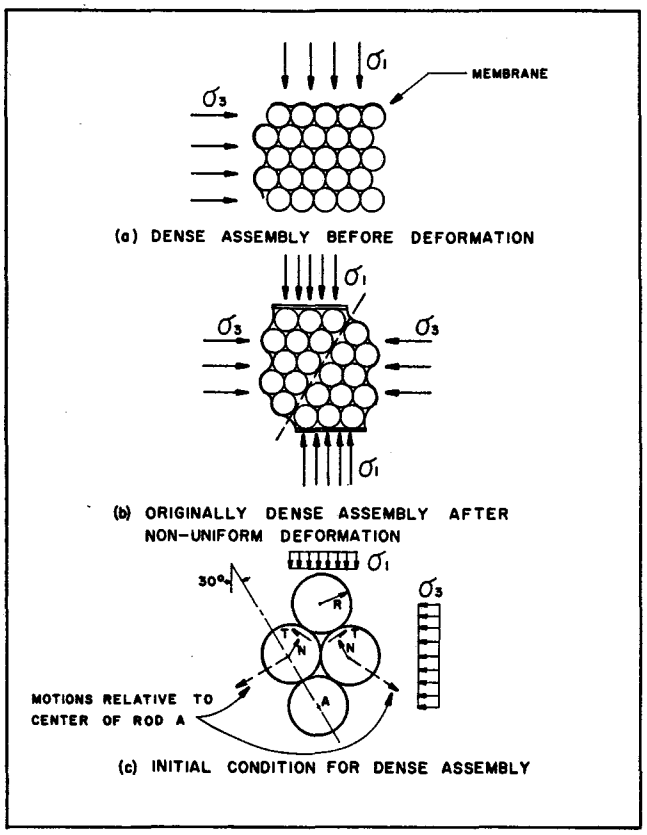

Figure 2-5. Axial compression of a dense assembly of rods (after Whitman, Ref. 37).

The theory of ideal granular material based on model studies has clarified certain points of this analysis. The following discussion is based on a recent publication by Rowe (Ref. 22), and a summary report by Whitman (Ref. 37). For cohesionless soils, a very much simplified model is considered. This model consists of a dense packing of rods, containing no liquid phase in the voids, as shown in Fig. 2-5. For the sake of simplicity, it is convenient to deal with the case of the dense packing. Figs. 2-5 (a) and (b) show the assembly before and after the vertical stress is increased. To aid in visualization, deformation is generally assumed to result only from gross sliding between particles, and elastic deformations are ignored. Therefore, once deformation starts, each rod is in contact with only four rods, and the system is statically determinate.

By analyzing the forces acting within the assembly, the normal N, and tangential T components can be written as follows:*

$$N = \frac{\sqrt{3}}{2} (\sigma_1 + \sigma_3) R \qquad (2\text{-}13)$$

$$T = \tfrac{1}{2} (\sigma_1 - 3\sigma_3) R \qquad (2\text{-}14)$$

respectively. Consequently, as the stresses acting are those at which slipping is incipient, Coulomb's law applies (see Eq. 2-3). The relationship for the maximum axial stress (σ_1) can be obtained by letting:

$$T = N \times f \text{ (Coulomb's law)} \qquad (2\text{-}15)$$

*See Appendix B.

where f = coefficient of friction, therefore Eq. (2-15) becomes

$$\tfrac{1}{2}\,(\sigma_1 - 3\,\sigma_3)\,R = f\left(\frac{\sqrt{3}}{2}\right)(\sigma_1 + \sigma_3)\,R$$

or

$$\sigma_1 = \frac{3 + f\sqrt{3}}{1 - f\sqrt{3}}\,\sigma_3 \qquad (2\text{-}16)$$

where f is the frictional coefficient applicable to sliding between two smooth surfaces.

It is of interest to observe that in Fig. 2-5 the horizontal component of the relative motion is greater than the vertical component. Hence, horizontal strains exceed vertical strains and the total assembly is expanding in volume. This volume expansion effect is termed dilatancy, which is the subject discussed in Section 2.4.3.

A theoretical and experimental investigation for several three-dimensional packing of spheres in triaxial compression has been made by Rowe (Ref. 22).

Let us now recall Eqs. (2-3) and (2-12). We have

$$\tau = (\sigma_3 - \mu)\tan\phi \qquad (2\text{-}3)$$

and

$$\sigma_1 = \frac{1 + \sin\phi}{1 - \sin\phi}\,\sigma_3 = \sigma_3 \tan^2\left(45° + \frac{\phi}{2}\right) \qquad (2\text{-}12)$$

Comparison of Eqs. (2-12) and (2-16) provides a relationship between f and ϕ. It was found that for the dense packing for steel rods, for which f was assumed to be 0.175, ϕ is found to be 40.6°.* The calculation indicates the importance of geometrical interference.

In summarizing the foregoing analysis, Eq. (2-16) constitutes a theory of the failure mechanism of a highly idealized granular material under certain stress conditions. The theory states, in general, that failure by slipping will occur on a particular surface when the ratio of shearing stress to normal effective stress on the surface reaches a certain maximum value. Actually, this failure theory was first suggested by Mohr as discussed in Section 2.3. Therefore, the treatment developed above also provides a theoretical basis for Mohr's theory.

It must be emphasized that no immediate general application to the failure of a real soil system is implied, for the behavior of a real material is much more complex than that assumed here. Nonetheless, the theory of ideal granular material is of value, since it shows in a clear, qualitative way: (1) the importance of geometrical interference in determining the friction angle at failure of the model for the array of rods as a whole, and (2) the cause and nature of the volume expansion which accompanies failure.

2.4.2 Pore-Water Pressure. The shear strengths of identical samples tested under undrained and drained conditions are, in general, quite different. This is due partly to the reduction of the shear strength caused by the pore-water pressure set up during an undrained test and partly to the increase in shear strength caused by the consolidation that takes place during a drained test.

However, in a dilatant soil, the pore-water pressure normally undergoes a slight increase at small deformation and then decreases as the soil grains tend to dilate. This decrease of pore-water pressure may be sufficient to produce significant negative values, and a point will then be reached at which bubbles of water vapor begin cavitation. This implies a departure from the fully saturated condition, and a further increase in deformation will not reduce the pore pressure below a limiting value at which the growth is able to continue.

In order to describe the development and characterization of pore-water pressure of saturated soils subjected to static loading, the pore pressure parameter, A, defined by the following expression has been found useful (Ref. 26).

$$A = \frac{\Delta\mu}{\Delta\,(\sigma_1 - \sigma_3)} \qquad (2\text{-}17)$$

where

$\Delta\,\mu$ = change in pore pressure

$\Delta\,(\sigma_1 - \sigma_3)$ = deviator stress increment

For the dense sand of Fig. 2-6, A reaches a value of −0.35 at the time of peak stress. The parameter A is affected by the details of loading and the properties of the material.

The development of pore-water pressure in an actual soil during the application of shear stresses is enormously complicated. In particular, the changes of pore-water pressure during rapid tests and influence of sample geometry upon such changes require further study. A

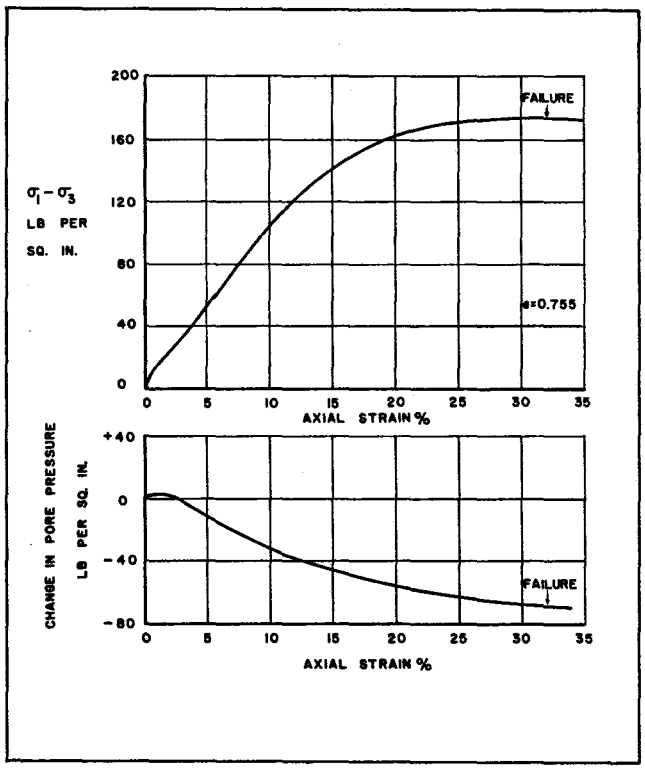

Figure 2-6. Consolidated-undrained test on saturated dense sand (after Bishop and Henkel, Ref. 2).

*If f = 0.175, as for clean steel surfaces, then $(\sigma_1)_f = 4.76\sigma_3$, by substituting $(\sigma_1)_f = 4.76\sigma_3$ into Eq. (2-12), we have $\phi = 40.6$.

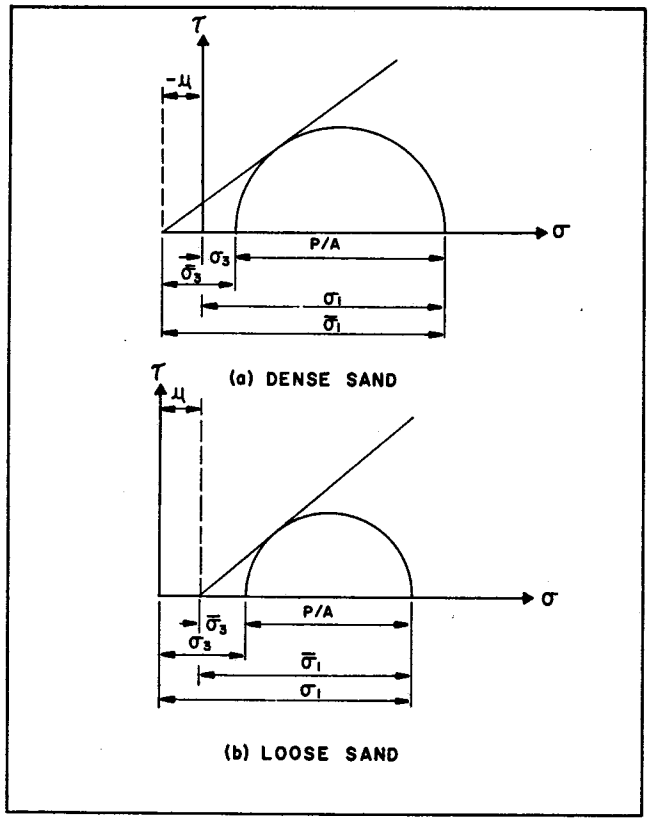

Figure 2-7. Effect of pore pressure generated in undrained triaxial test on saturated sand.

limited study of pore-water pressure as it influences dynamic load is included in this investigation.

Neglecting dynamic effects, we can study the pore-water pressure developed in a cohesionless soil specimen with reference to Mohr's theory. As was stated in Eq. (2-8), the effective confining stress in a saturated soil-water system can be considered as the algebraic difference of the applied confining pressure and the specimen pore-water pressure. Thus we have

$$\bar{\sigma}_3 = \sigma_3 - \mu$$

where $\bar{\sigma}_3$ is the effective confining pressure, σ_3 is the applied confining pressure and μ is the pore-water pressure (see Fig. 2-7).

Eq. (2-12) can be written in terms of effective stress, and $\bar{\sigma}_1$ can become $\left(\bar{\sigma}_3 + \frac{P}{A} \right)$. If this is done, the following equation is obtained. (See Fig. 2-7).

$$\bar{\sigma}_3 + \frac{P}{A} = \bar{\sigma}_3 \tan^2 \left(45 + \frac{\phi}{2} \right) \quad (2\text{-}18)$$

Eq. (2-18) can be solved for $\frac{P}{A}$ giving

$$\frac{P}{A} = \bar{\sigma}_3 \left[\tan^2 \left(45 + \frac{\phi}{2} \right) - 1 \right] \quad (2\text{-}19)$$

Substituting Pw for P and $(\sigma_3 - \mu)$ for $\bar{\sigma}_3$ in Eq. (2-19) yields

$$\frac{Pw}{A} = (\sigma_3 - \mu) \left[\tan^2 \left(45 + \frac{\phi}{2} \right) - 1 \right] \quad (2\text{-}20)$$

where Pw is designated the ultimate load applied to the saturated specimen.

In the case of a dry "drained" specimen, however, the magnitude of pore-water pressure must become zero. Eq. (2-19) for the dry "drained" specimen can be expressed as follows:

$$\frac{Pd}{A} = (\sigma_3 - 0) \left[\tan^2 \left(45^\circ + \frac{\phi}{2} \right) - 1 \right] \quad (2\text{-}21)$$

Hence, if Eqs. (2-20) and (2-21) are solved simultaneously for μ, one can obtain an expression for the pore-water pressure, μ, in terms of Pw, Pd and the parameter (ϕ):

$$-\mu = \frac{Pw - Pd}{A \left[\tan^2 \left(45^\circ + \frac{\phi}{2} \right) - 1 \right]} \quad (2\text{-}22)$$

It should be pointed out that the principle of superposition as well as constant angle of internal friction were assumed in the above derivations. Schematic diagrams showing such conception are illustrated in Fig. 2-8.

2.4.3. Dilatancy Component. A third factor in the behavior of soils under stress is their volumetric change during shearing, a phenomenon which was first referred to by Reynolds (Ref. 21), as dilatancy or dilation.

This phenomenon has been described and analyzed by Taylor (Ref. 30) and Bishop (Ref. 2). Some of the basic considerations on this subject matter follows:

If Eq. (2-3) is rewritten in terms of the ratio of stresses acting on the failure plane of Mohr's circle, it is seen that the contribution due to friction can be determined. Therefore, Eq. (2-3) can be written in a functional form:

$$\tau_f = \bar{\sigma}_f \tan \phi = F_1(f,G)$$

or

$$\frac{\tau_f}{\bar{\sigma}_f} = \tan \phi = F_2(f,G) \quad (2\text{-}23)$$

in which the subscript f refers to conditions on the failure plane; f and G are frictional and geometrical factors, respectively. If a test is performed in which τ_f, the shear stress on the failure plane required for failure to occur, is measured for a given normal stress, σ_f, and an estimate can be made of that proportion of the shear stress which goes into dilating the soil against the normal stress, then, according to Gibson (Ref. 10), the remaining shear stress can be attributed to grain-to-grain frictional effects. However, this measurement would be difficult to make with a triaxial test on soil, and Gibson, therefore, used a direct shear test in which the measure-

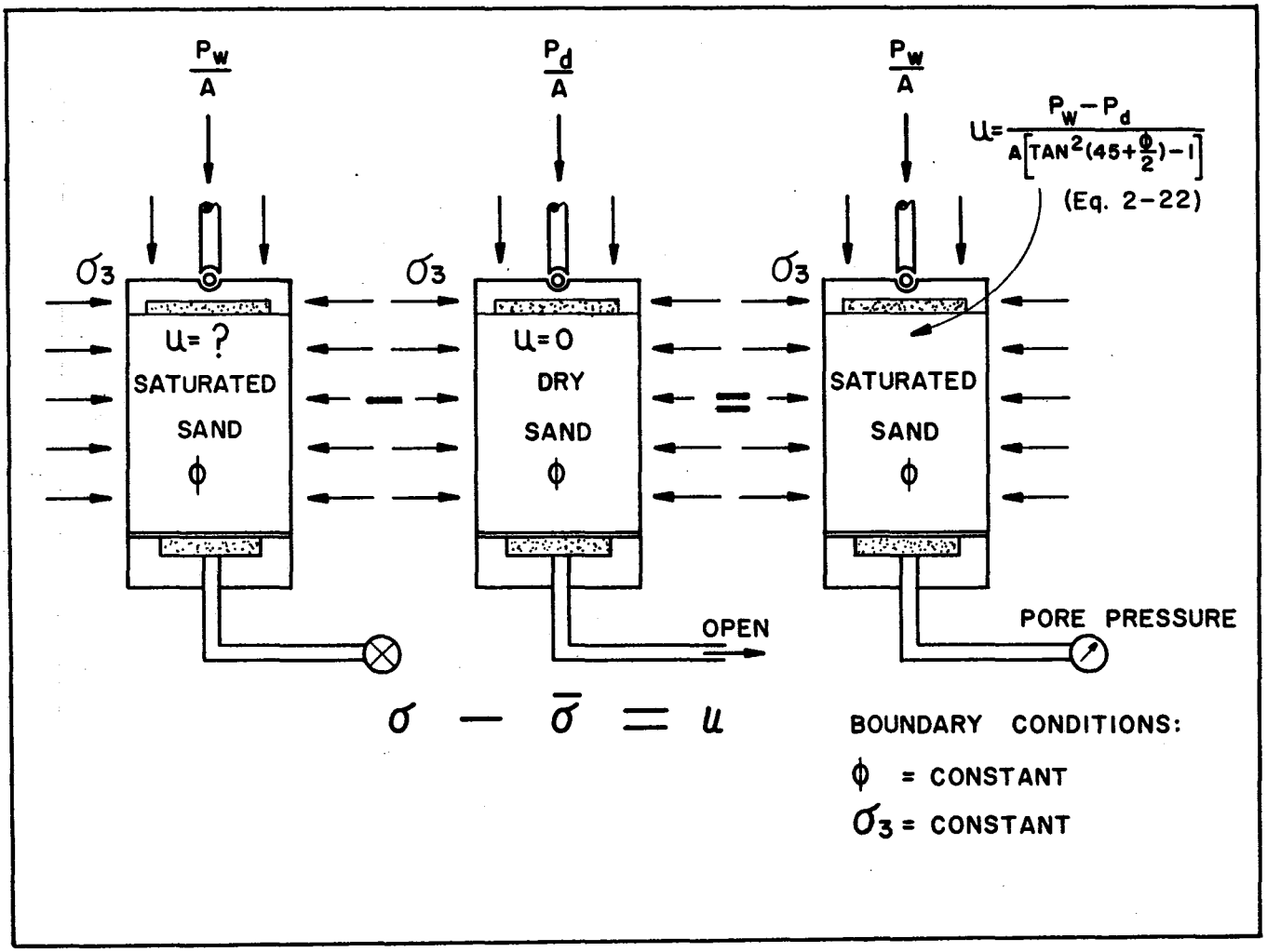

Figure 2-8. Indirect measurement of pore-water pressure.

ment of gradient at failure was obtained from the curve of the increase in thickness of the sample, V, verus shear displacement, S. Thus, he assumes that

$$\frac{\tau_f}{\bar{\sigma}_f} = \tan\phi = \tan\phi_f + F(G) = \tan\phi_f + \left(\frac{\partial V}{\partial S}\right)_f \quad (2\text{-}24)$$

In soils, the geometrical factor is reflected in the grain size, shape, distribution, and in the void ratio; but for any one soil, any variation which occurs will take place in the void ratio and in the structure of the soil. Thus, an investigation of the value of $\left(\frac{\partial V}{\partial S}\right)_f$ in Eq. (2-24) will give an indication of the effect of the geometrical parameter in addition to the contribution of the intergranular friction coefficient to the shear strength of the soil.

In an undrained triaxial test, the pore-water pressure caused by the dilation of change in volume of the sample is μ, the axial and lateral principal total stresses σ_1, and σ_3, respectively. The major and minor principal *effective* stresses are:

$$\bar{\sigma}_1 = \sigma_1 - \mu \quad (2\text{-}25)$$

and

$$\bar{\sigma}_3 = \sigma_3 - \mu \quad (2\text{-}26)$$

respectively, and the normal effective stress on any plane in the sample is:

$$\bar{\sigma} = \sigma - \mu \quad (2\text{-}27)$$

The high permeability of granular soils causes a uniform excess pore pressure throughout the sample, although the volumetric changes in the soil are usually not uniform because of the end restraint of the sample. The effect of the pore pressure generated in an undrained test on dense and on loose samples at failure is illustrated by the Mohr diagrams shown in Fig. 2-7. The total principal stresses at failure are plotted along the σ-axis from the origin O, and the stress circles are drawn with the principal total stresses difference as the diameters.

In a natural sand deposit, conditions of both rapid stressing due to pile driving or earthquakes and built up in negative pore pressures can occur. Under these circumstances, the effective stresses in a dense saturated sand deposit increase, and the material exhibits a considerably enhanced resistance to failure. In loose, saturated sands, however, the effective stresses are reduced by rapid shearing, and the grains may even lose contact with one another entirely for short intervals of time. The effective shear strength of the loose condition is greatly diminished since the mass of soil affected becomes almost entirely fluid. If the positive pore pressure is increased to the point that effective stress is reduced to zero, the sand is said to liquify.

Chapter III

PRINCIPAL FEATURES OF THE TESTING MACHINES AND TRIAXIAL APPARATUS

3.1. Static Loading Apparatus

Static loading apparatus may be classified into two types; namely, controlled rate of load application or controlled rate of deformation. Chen (Ref. 6) found that the results of strength tests on sand are practically identical, regardless of whether the test is performed with load control or deformation control. However, deformation control is found more favorable because the peak value of strength is obvious during the test.

A geared loading apparatus by Soiltest was used in this investigation. This apparatus is as shown in Fig. 3-1. To perform a loading test with this apparatus, the test specimen is placed on the loading base, and the loading base is raised until the top cap contacts the proving ring. The motor-driven drum is then started, producing a constant, slow, upward movement of the loading base. Load was measured by a load cell, and axial deformation by a displacement transducer, both of which were recorded by oscilloscope as described in Section 4.3.

The rate of deformation during a test was 0.05 in. per minute.

3.2. Dynamic Loading Apparatus

In general, for performing dynamic loading tests, either a controlled impulse method or a controlled deformation method may be used. In the controlled impulse method, the specimen is subjected to an impulse loading by a falling weight, whereas in the controlled deformation method the specimen is subjected to a constant rate of axial deformation.

The basic requirement imposed upon the test equipment is the capacity of performing triaxial compression tests upon the test specimen at various rates of loading. The static test (conventional laboratory triaxial compression tests) requires several minutes or even several hours for completion (Ref. 2). A time to failure of about 0.01 second was desired to simulate pile driving conditions.

In order to meet these objectives, it was decided that the equipment must be *simple* and *reliable* in opera-

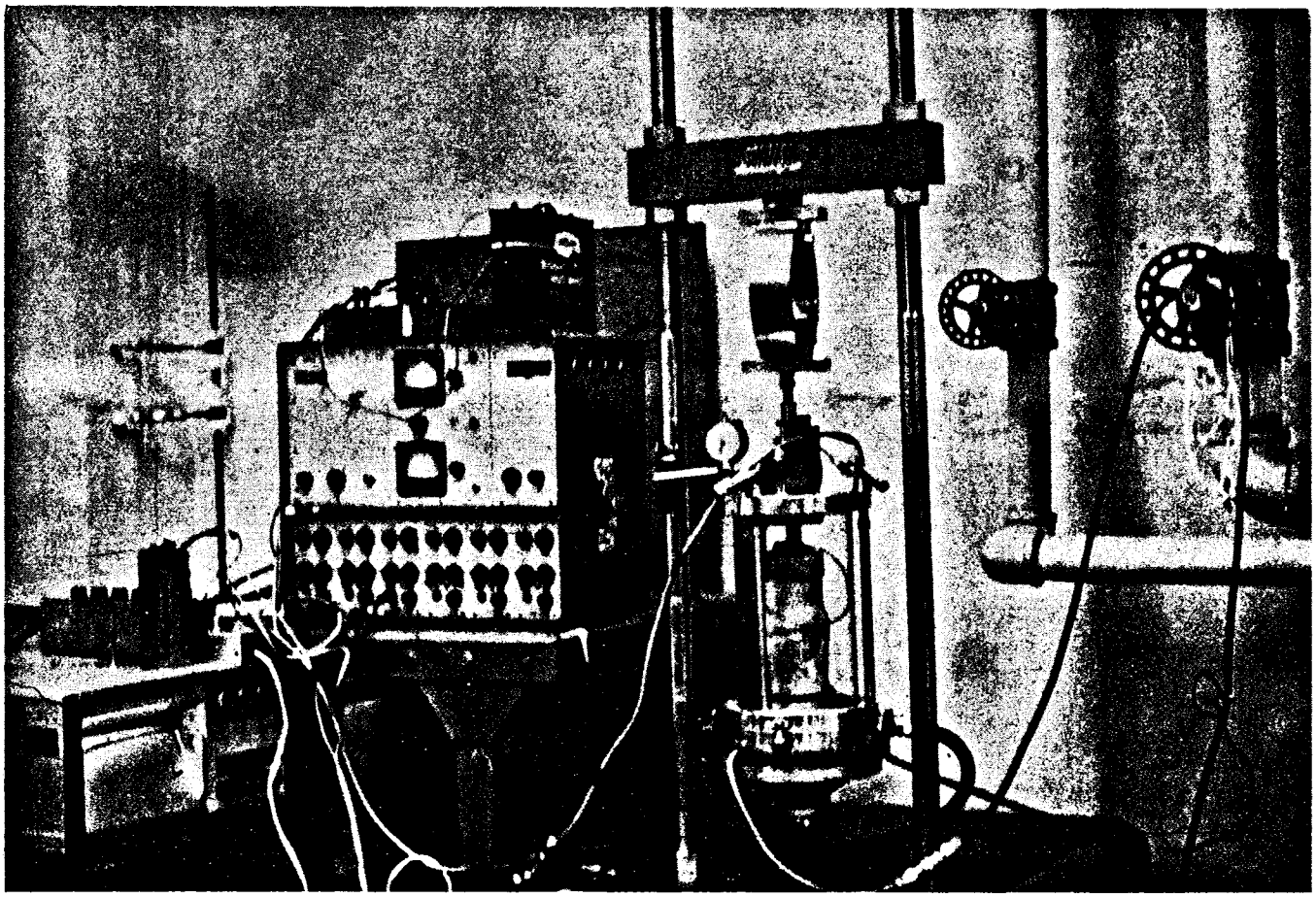

Figure 3-1. Static loading apparatus setup.

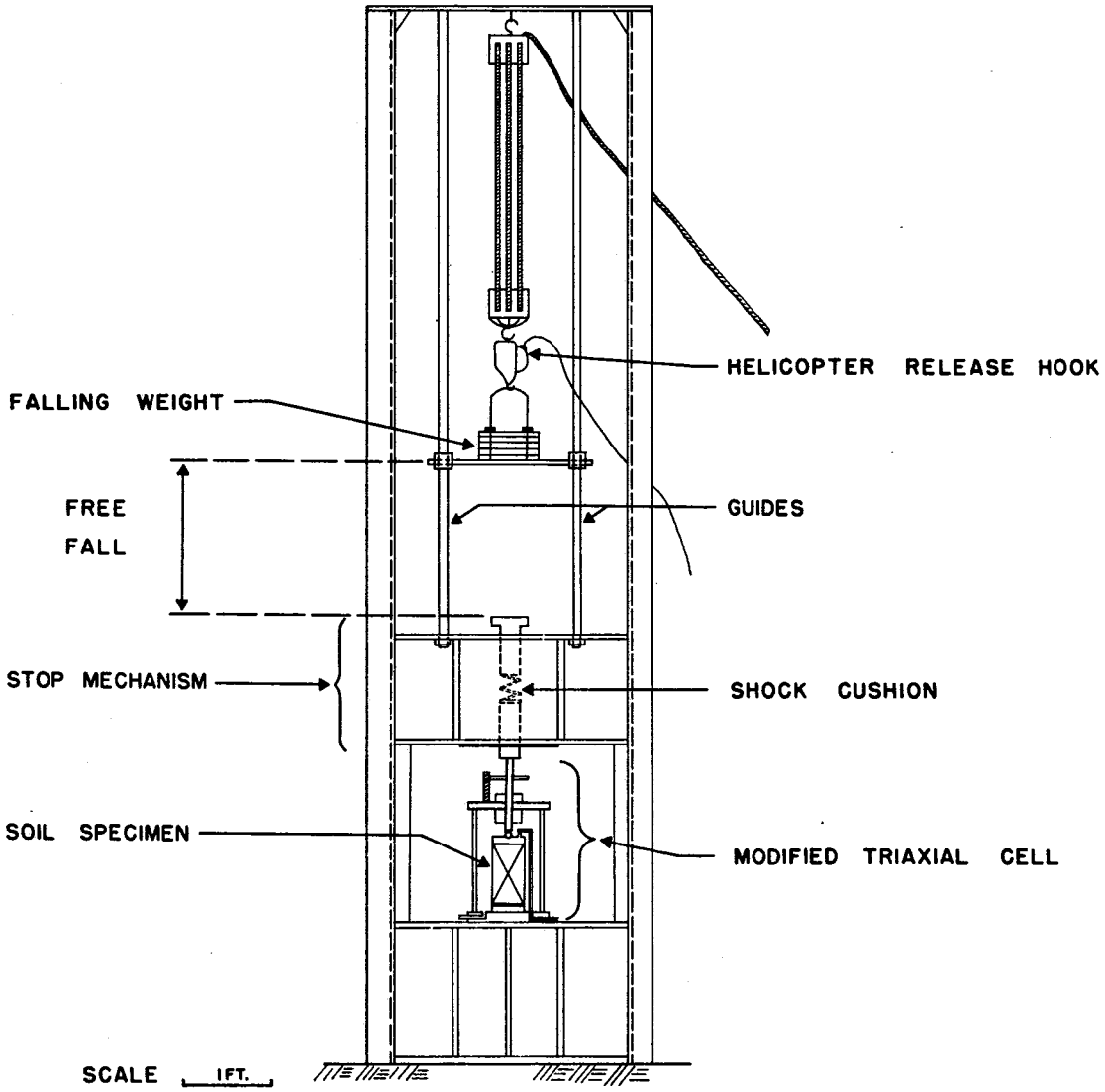

Figure 3-2. Dynamic loading apparatus.

tion. Consequently, a controlled impulse method was used in this investigation.

This loading apparatus, illustrated in Fig. 3-2, consists of a falling weight, stop mechanism, shock cushion, etc. The dynamic instrumentation set-up is shown in Figs. 3-2 and 3-3. A block diagram of the dynamic instrumentation is shown in Fig. 3-4.

As described in the preceding paragraphs, the load is applied by a heavy weight which, as it falls through space, contacts the piston of the triaxial cell. Because of the large mass of the falling weight, the velocity of the load piston will be substantially constant during the interval that force is applied to the soil sample.

Four different loading rates (or velocity of the falling weight), 48.3 in. per sec., 83.6 in. per sec., 118.0 in. per sec.* and 0.00083 in. per sec. (0.05 in. per min.), which are representative of pile velocities measured during driving, were used in this investigation.

The weight was guided during the fall along the desired vertical line by two guide rods. The guide rods were 1 in. diameter by 40 in. long, Thompson R60C precision hardened and ground shafts. Thompson sleeve-type roller bearings were mounted on the weight slide, and the resulting friction force was reduced to a mini-

*The numerical values were based on the free-falling of 3 in., 9 in., and 18 in., respectively.

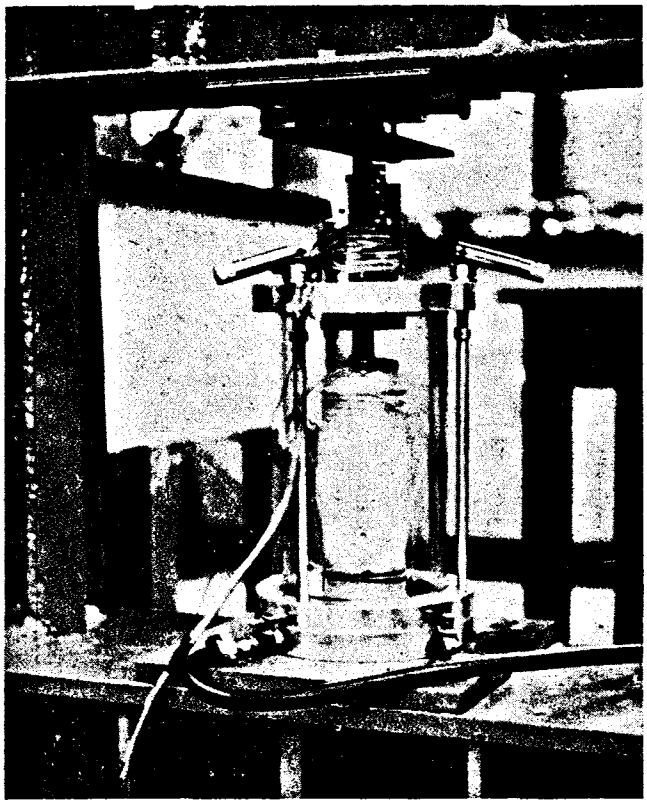

Figure 3-3. Close-up of triaxial cell and specimen after failure.

mum. A 120 lb. falling weight was used, and drop heights of 3 in., 9 in., and 18 in., were used to obtain the desired velocities.

A stop mechanism was provided for bringing the falling weight to a halt after it had imposed the necessary strain upon the specimen. The stop mechanism was located over the loading piston in the triaxial cell.

A helicopter release hook was provided for hoisting the weight back up to its elevated position prior to and following a test. This release device could be operated either manually or electrically.

3.3. Modified Triaxial Cell

As discussed in Section 2.1, the triaxial test was considered the most desirable for studying dynamic strength characteristics of soils. The triaxial cell used was one made by Texas A&M University, which had been modified with a load cell in its base. Fig. 3-3 shows a close-up view of the modified triaxial cell and a failed specimen.

The load measuring device or load cell was located within the triaxial chamber at the bottom of the sample as shown in Fig. 3-5. This device took the place of the pedestal on which the sample rested. It thus measured the load at the base of the specimen and minimized the inertia effect of the upper loading components which were in motion.

The load cell (Fig. 3-5), rated approximately at 2000 lb. capacity, was made of a 2.875 in. outside diameter hollow aluminum (TS6061-TG) cylinder with a 0.093 in. thick wall. The cell was equipped with four Type C-6-121-R2TC Budd Metalifilm strain gage rosettes attached inside the wall of the cylinder. Two of these gages were vertical and were arranged opposite each other to the axis of the cylinder. The other two gages were perpendicular to the axis of the cylinder. All gages were attached with epoxy cement and were air dried for several hours after attachment before being placed in an oven at 60°C. Immediately upon removal from the oven, the gages were coated with Gagekote #3 for moisture proofing. A photograph of the load cell is shown in

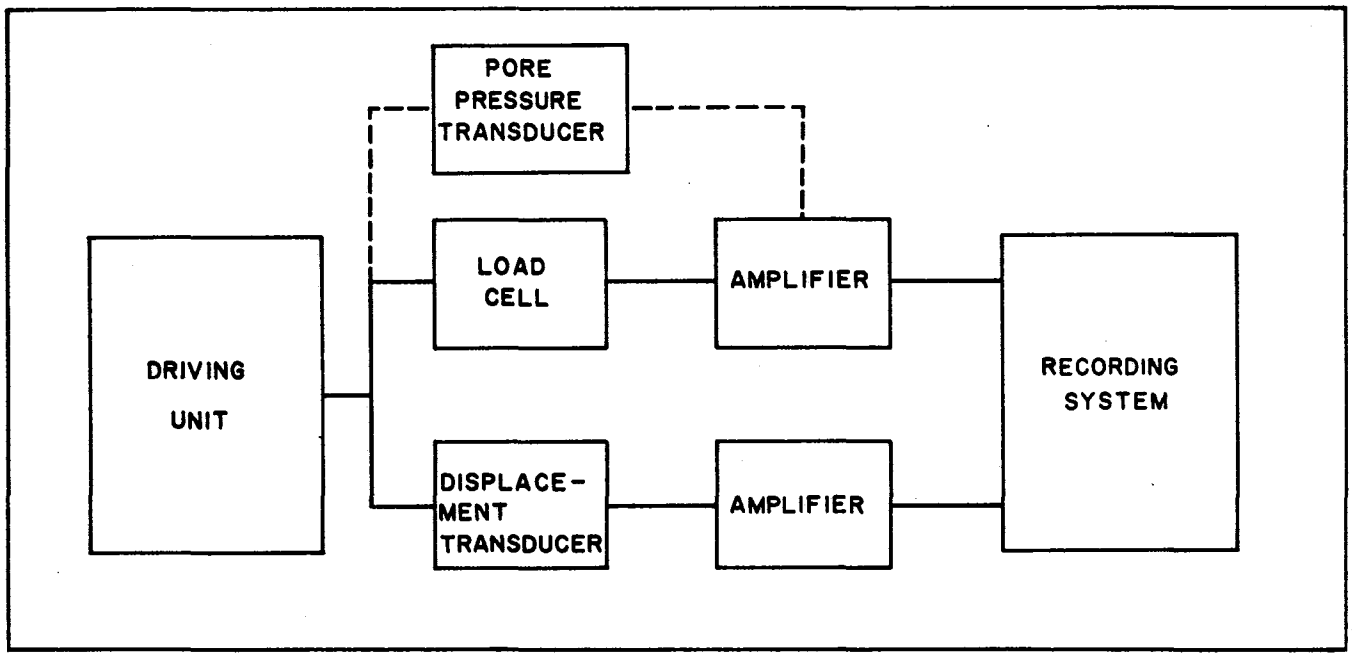

Figure 3-4. Block diagram of the dynamic instrumentation setup.

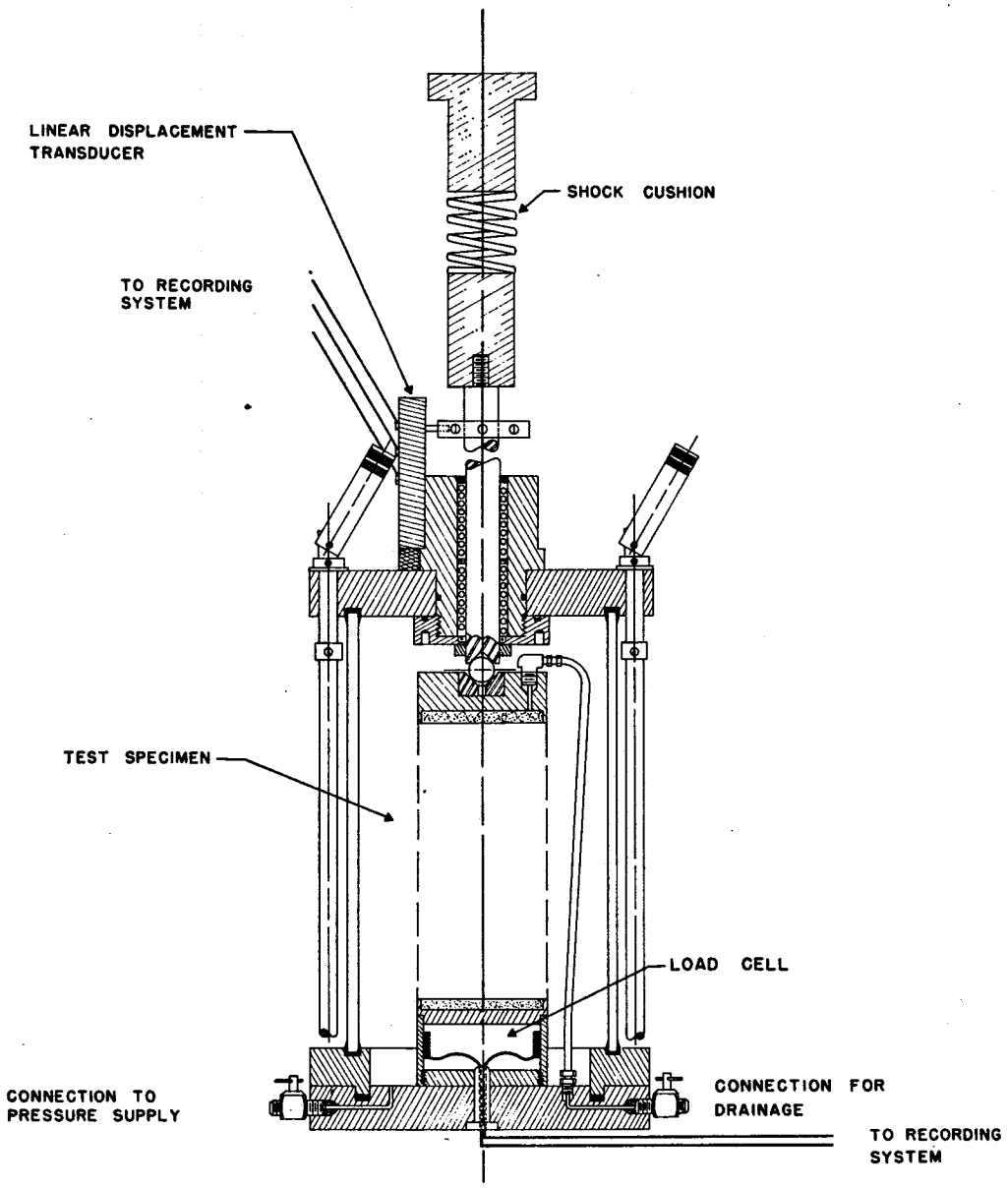

Figure 3-5.

Fig. 3-6,* and a diagram of the wiring arrangement is shown in Fig. 3-7.

The deformation of the sample was measured by a linear displacement transducer which detected the motion of the loading piston of the triaxial cell. The unit was a wire resistance type potentiometer manufactured by Boerns Electronics. The electric circuit of the system was as shown on Fig. 3-8. The maximum range of the transducer was 0.934 in. It had a sensitivity of 0.003 in.

A shock cushion (spring) was provided between the hammer and the top of the loading piston of the triaxial compression device as shown in Fig. 3-5. This cushion was used to reduce the shock acceleration force on the lower loading piston and soil sample. The falling weight first contacts the upper loading piston, and it compresses the spring which exerts an increasing force on the lower loading piston. This force accelerates the lower loading piston in such a way that it quickly attains a constant velocity.

*It is necessary to point out that the load cell originally designed for use with the dynamic testing equipment was found leaking at the connection of drainage channels, and the maintenance procedure was complicated. It was, therefore, suggested to seal these drainage channels. Since this series of tests, several variations of the "new" basic load cell have been constructed.

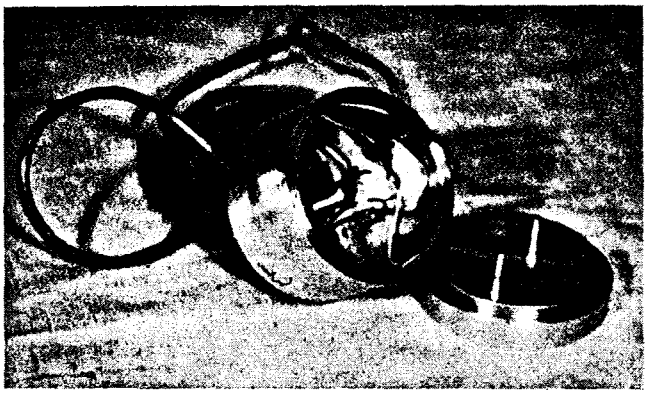

Figure 3-6. Load cell.

The pore pressure gage used was a Type 4-312, 0.5 in. diameter, electrical pressure transducer manufactured by Consolidated Electrodynamics Corp. of Monrovia, California. It has a pressure range from 0 to 100 psi and is temperature compensated over a range of −65° to 165°F. Such an assembly is represented in pictorial and schematic form in Fig. 3-9. Fundamentally, the element is a mechanical device which is designated to cause a controlled (magnitude and direction) strain application to the strain gage windings.

The pressure to be measured causes displacement of the diaphragm. A force rod connected to the center of the diaphragm transmits the force (proportional to the applied pressure) to the sensing element. The sensing element is a spring structure which supports the strain gage wire windings. Movement of the center of the spring causes movement of the posts upon which the strain windings are mounted, thus increasing the strain (and resistance) of the windings at one end of the posts while decreasing it at the other end.

The windings, in the form of a four-active-arm Wheatstone Bridge, provide an output that is a linear

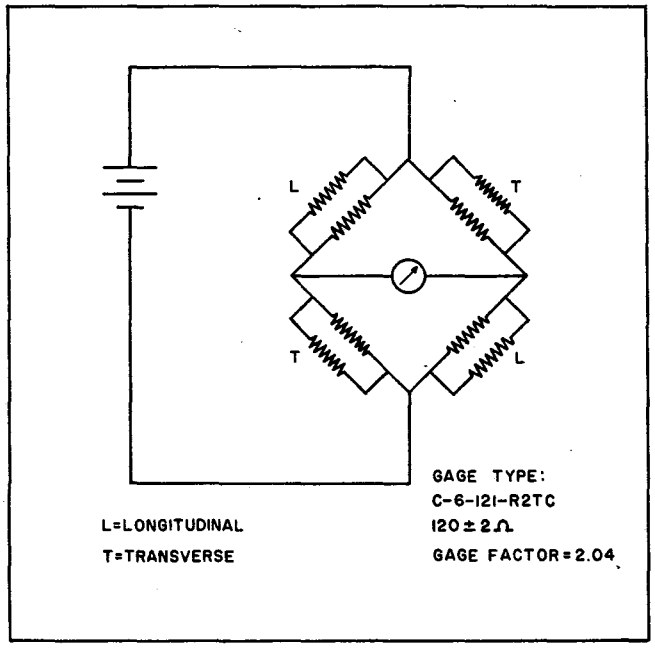

Figure 3-7. Load cell circuit.

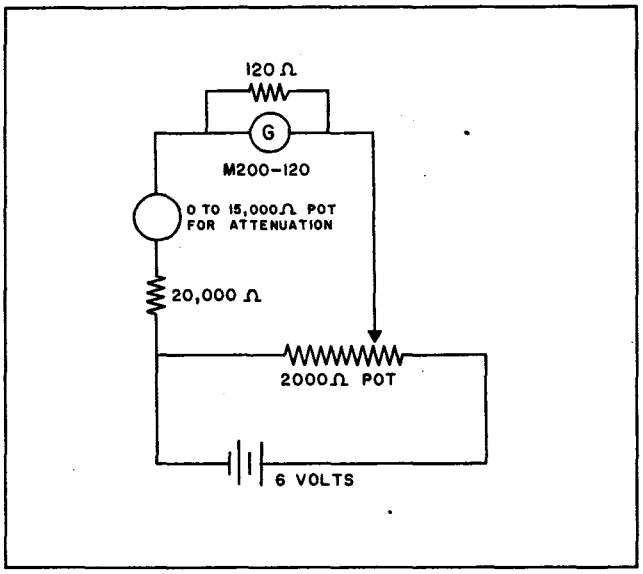

Figure 3-8. Linear displacement transducer circuit.

function of the magnitude of the pressure applied to the diaphragm.

To house the pressure transducer, a clear lucite holder was provided. The walls were 0.375 in. thick so that volumetric change of the housing was very small under the pressures encountered. The housing is at-

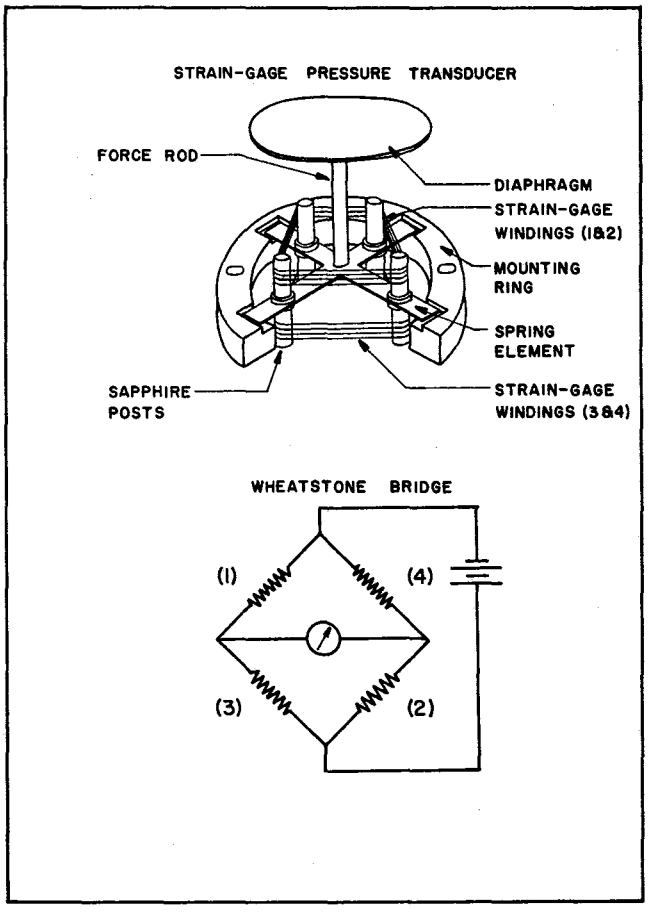

Figure 3-9. Schematic diagram of pressure gage.

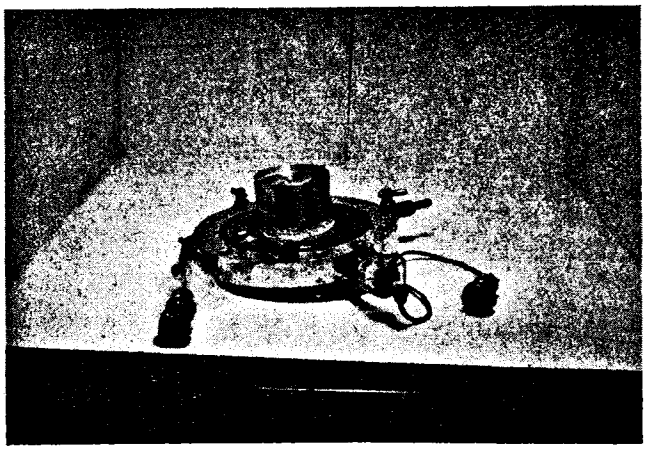

Figure 3-10. Triaxial compression cell base with pore-pressure transducer.

tached directly to the Circle Seal valve leading to the triaxial cell base, and it was provided with a port for bleeding off any air bubbles which collected in the measuring system. Fig. 3-10 shows a photograph of the system.

3.4. Recording System

A Honeywell Model 1508 Visicorder Oscillograph and a Model 119 Carrier Amplifier System, as shown in Fig. 3-11, were used to record all experimental results.

The oscillograph Visicorder, an electrical-optical-mechanical precision instrument, records data photographically on a moving strip of photographic paper (Kodak Linagraph Direct Print Paper). A light beam moves laterally at a rate and amplitude proportional to some time interval of interest and exposes the photographic film. When the photographic paper is developed, the permanent image of the light beam can be measured, and with the proper scale factor the physical quantity can be determined.

The most important part of the oscillograph is the galvanometer. The rotation of the galvanometer mirror provides the rate and amplitude of the light source.

The timing system was independent of the recorded speed, and the space between two time lines always represents the same increment of time. During recording, this time-marking device produced time lines at the desired interval of 0.01 seconds on the paper. The paper speed was normally run at 80 in. per sec. (See Fig. 3-12 for a typical record run.)

3.5. Calibration of Equipment

The load cell was calibrated statically in a consolidation machine and an Instron machine by applying loads at 100 lb. increments and recording the load cell output on the recording oscillograph. The load versus trace displacement of the oscillogram was plotted directly as shown in curves A and B in Fig. 3-13. A calibra-

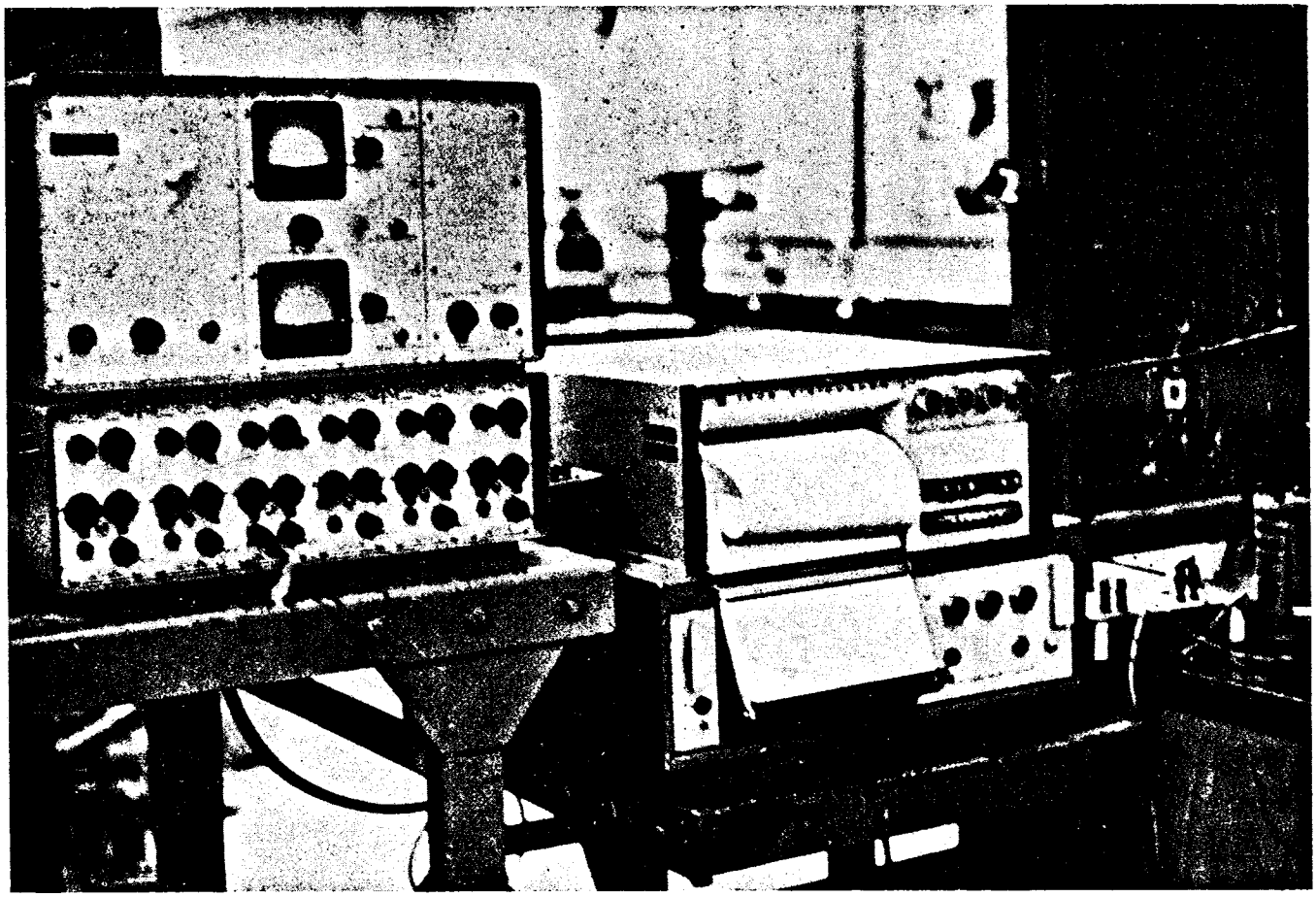

Figure 3-11. Recording equipment.

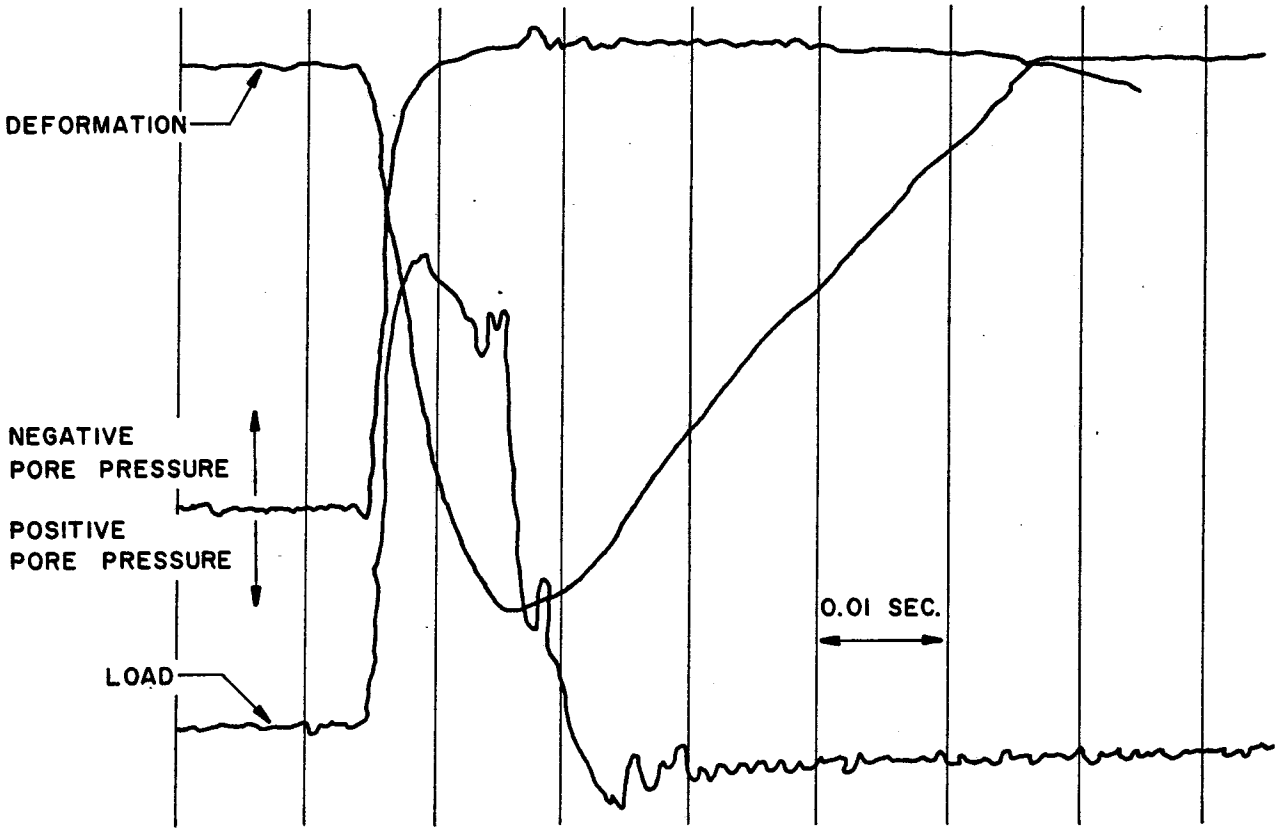

Figure 3-12. Typical oscillogram of load-deformation-pore pressure data.

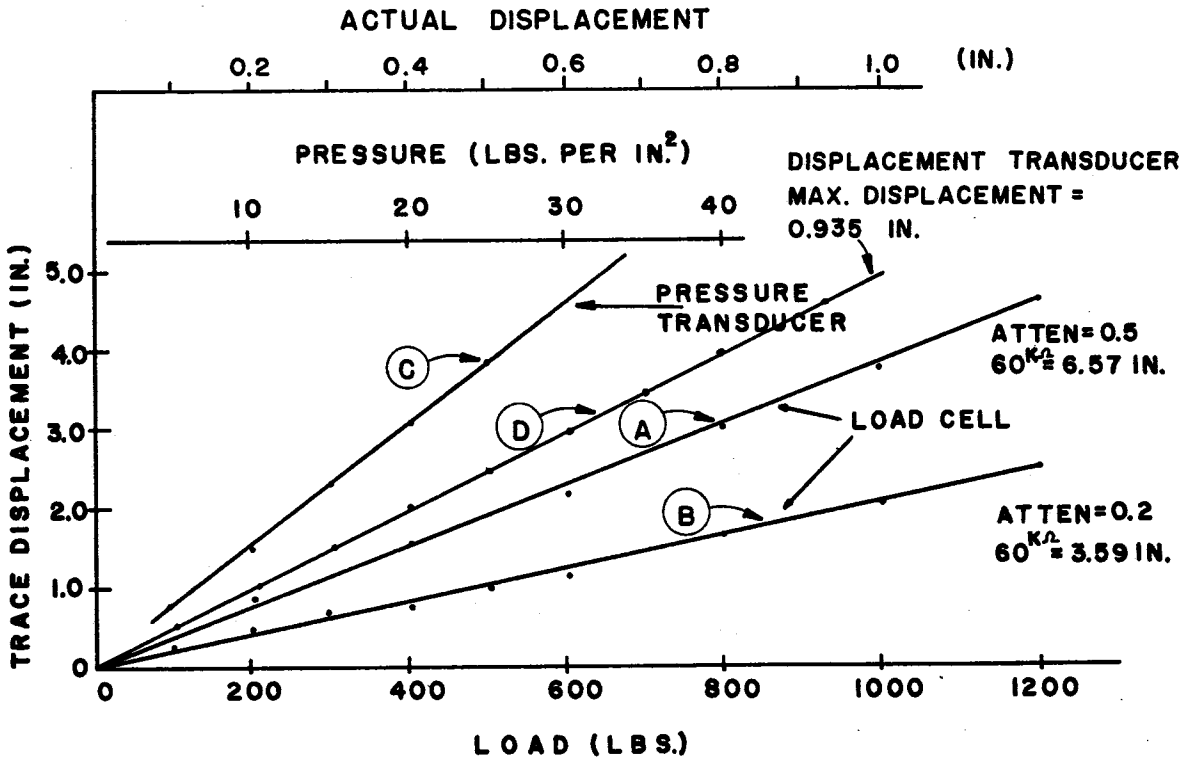

Figure 3-13. Calibration curves.

tion resistor of 60,000 ohms in the bridge balancing unit allowing the balance unit to be reset at various times so that the output of the record remained constant. The calibration constant for the load cell was found to be

0.0286 lb. per ohm $\left(= \frac{1720 \text{ lb.}}{60{,}000 \text{ ohm}} \right)$.

The calibration of pore pressure was made by applying known pressure and recording the pressure transducer output on the recording oscillograph. The pressure versus trace displacement of the oscillogram was plotted directly as shown in curve C in Fig. 3-13. The calibration constant for the pressure transducer was found to be

0.00533 psi per ohm $\left(= \frac{32.2 \text{ psi}}{60{,}000 \text{ ohm}} \right)$.

The linear displacement transducer was calibrated by means of an Ames dial gage to measure the actual displacement of the displacement transducer and record the output on the recording oscillograph. A typical calibration curve for the displacement transducer is shown in curve D in Fig. 3-13.

Chapter IV

LABORATORY PROCEDURE AND PROGRAM

4.1. Description of Soils Tested

The major portion of tests on cohesionless soils in this program was performed on standard Ottawa sand. A few tests on a fine sand from Victoria, Texas were also tested as part of the research program.

Ottawa Sand—Standard 20-30 Ottawa sand is a rounded granular material composed of more than 90 per cent quartz, with a uniform grain size distribution as shown in Curve A of Fig. 4-1.

Victoria Sand—This sand is a natural sand deposited in a sedimentary bed in Victoria, Texas. The 10 foot

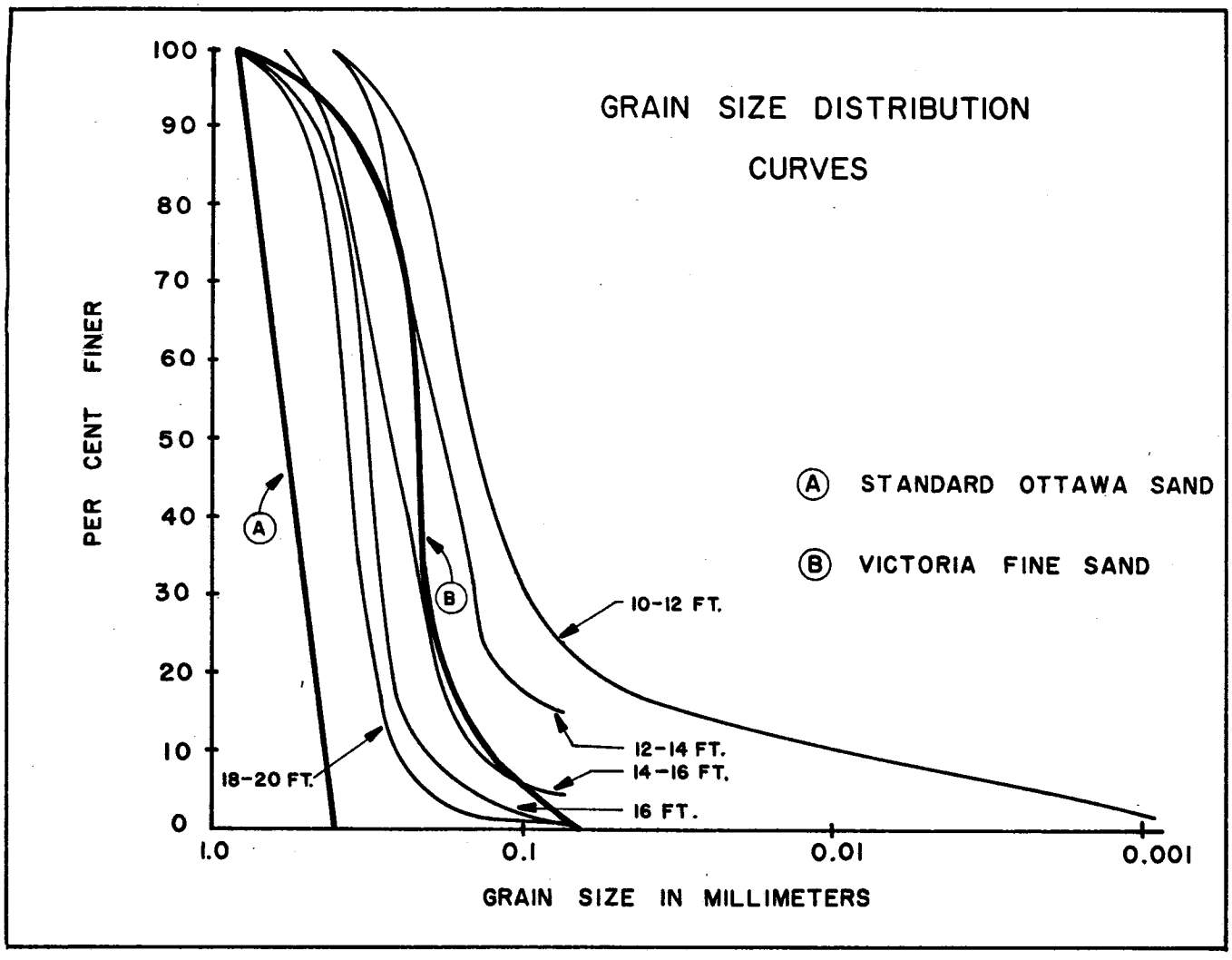

Figure 4-1.

thick sand deposit underlies a clay bed that is 10 feet thick. Grain-size distribution curves of various depths are also shown on Fig. 4-1. In working with the soil, it was observed that the small and large particles tended to segregate from each other, and this state of affairs led to extreme difficulties in the preparation of homogeneous test samples and in the duplication of sample properties from one specimen to the next. It was, therefore, necessary to combine the total sample and to wash it through the No. 200 sieve. The actual grain size distribution for the samples tested is shown as Curve B in Fig. 4-1.

4.2. Preparation of Test Specimen

In order to make a sand specimen for use in the triaxial test, it is necessary to use a forming mold which will maintain the required specimen shape until effective stresses of sufficient magnitude to make the specimen self-supporting can be applied.

Complete saturation is extremely difficult to obtain if the sample is placed dry and, subsequently, flooded. In a series of preliminary tests, attempts to obtain a high degree of saturation were made by starting with a dry sample. In this method, the weight and the void ratio of the sample were computed from the dimensions of the specimen. After a specimen of oven-dry sand had been compacted inside the membrane, it was bound to the pedestal. The vacuum pressure was then applied to the interior of the specimen, and the mold supporting the membrane was removed. Theoretically, this procedure is ideal due to the fact that the entire system is a closed one. However, complete saturation requires a complete interior vacuum which is very difficult to obtain in the test specimen.

These difficulties can be avoided by depositing the sand under water. Similar procedures were suggested by Bishop and Henkel (Ref. 2) and Whitman and Healy (Ref. 38). The following paragraphs give a more detailed account of the method used.

Prior to each test, the porous disc was soaked in demineralized water to insure a complete saturation of the system. A Carrol Warren 2.8 in. diameter membrane was used on the lower pedestal of the triaxial device and fastened with a rubber O-ring. A forming mold made of aluminum was then clamped around the membrane. The membrane was filled to within one inch from its top with demineralized water.

The void ratio of the test samples was computed from the sample volume, V, and the volume of the sample solids, Vs, according to Eq. (4-1).

$$e = \frac{V}{Vs} - 1 \qquad (4\text{-}1)$$

In order to obtain the desired initial void ratio of the test sample, the weight of the sand and the volume of the mold must first be calculated. The sand was then saturated by mixing it in a beaker with enough demineralized water to cover the sand. The mixture was tamped to remove trapped air. The sand was deposited through water and vibrated by means of gentle taps with a rubber hammer. The sand in the membrane was brought up to the desired height and leveled off. The water level was just at the top of the membrane at this point, and the top pedestal was pushed down through the water on the sand. Consequently, the hose from the top pedestal to the base was also filled with water. Therefore, the whole system was saturated. This required a certain degree of skill developed through experience.

Table 4-1. Initial Tests of Degree of Saturation

Test No.*	Initial Void Ratio e_o	Applied Lateral Pressure (psi)	Recorded Pore-Water Pressure (psi)	Computed Degree of Saturation %
pw-2B	0.50	5.0	4.90	98.0
		10.0	9.8	98.0
pw-5	0.60	5.0	4.95	99.0

*A complete list of tests is given in Table 4-2.

A slight suction was obtained by lowering a burette which was physically connected to the sample base, thereby giving rigidity to the sample. The forming mold could then be removed. The triaxial chamber cover was put in place and the chamber pressure applied. At this point, the valve to the burette was closed.

Two specimens were investigated to check the degree of saturation with the above mentioned procedure. It was found that the specimens ranged from 98.0% to 99.0% saturation.

According to Eq. (4-2)* (See Table 4-1):

$$\delta\mu = \delta\sigma_3 \qquad (4\text{-}2)$$

Where $\delta\mu$ = the change in pore-water pressure for a 100% saturated sample.

$\delta\sigma_3$ = the change in lateral confining pressure.

This was judged satisfactory for the present purpose.

4.3. Pore-Water Pressure Measurements

An understanding of why different rates of loading produce different peak strengths comes from a study of the pore-water pressure changes which develop in the cohesionless soil during undrained tests.

The method for measuring pore-water pressure during a triaxial compression test involves the use of a pressure transducer. The principle of the pressure transducer measurement has been explained in Section 3.3 of this study. A more detailed procedure for the pore-water pressure measurement by means of a pressure transducer is described in the following paragraphs.

Despite the difficulties introduced by the leakage of the drainage channels of the load cell as described in Section 3.2, the pore-water pressure was measured at the base of a conventional triaxial cell by means of a pressure transducer Type 4-312 as shown in Fig. 3-9. The pore-water pressure measurement was then superimposed on the load-axial deformation measurement as shown in Fig. 3-12.

*See Appendix C.

In all of these tests, once the porous stone and the base pedestal drainage channels were saturated, a supply of demineralized water was connected to one of the base pedestal drain valves. The pressure transducer was connected to the remaining pedestal drain valve. Water entered the transducer housing from the water supply and forced all of the air through the bleed valve of the housing. Once the system appeared to be saturated, the bleed valve was closed but the water supply valve was left open. If there were no visual signs of air bubbles, the water supply valve was closed. Following the above procedure, test specimens were prepared according to Section 4.2.

4.4. Laboratory Program

The laboratory program consisted of both static and dynamic tests. The static tests were performed at a strain-rate of 0.05 in. per minute on a Soiltest compression testing machine. The dynamic tests were divided into three groups based upon the rate of loading. They were nominally: (1) 40 in. per sec., (2) 80 in. per sec., and (3) 130 in. per sec. All dynamic tests were conducted with the same apparatus. The deformation rate was adjusted by varying the heights of free fall.

Tests on Ottawa sand and Victoria sand were performed in this research program. The complete testing program is tabulated in Table 4-2. For convenience, the following symbols have been adopted for identifying the characteristics and conditions of the tests:

Symbol	Term
O	Ottawa Sand
V	Victoria Sand
S	Saturated State
D	Dry State
U	Undrained Condition
R	Drained Condition
PW	Pore-Water Measurement

For example, the symbols OSU and VSR in Table 4-2 refer to the tests of saturated undrained test on Ottawa sand and saturated drained test on Victoria sand, respectively. In the next chapter (Chapter V), data from the above mentioned test program will be discussed in detail.

TABLE 4-2. TRIAXIAL COMPRESSION TEST PROGRAM

Test No.	Soil Type	e_0 Initial Void Ratio	σ_3 Lateral Confining Pressure (psi)	Height of Drop (in.)	Test Conditions
OSU-1	O	0.50	45.0	18	SU
OSU-2	O	0.50	30.0	18	SU
OSU-3	O	0.50	15.0	18	SU
OSU-4A	O	0.50	45.0	9	SU
OSU-4B	O	0.50	45.0	9	SU
OSU-5	O	0.50	30.0	9	SU
OSU-6	O	0.50	15.0	9	SU
OSU-7	O	0.50	45.0	3	SU
OSU-8	O	0.50	30.0	3	SU
OSU-9	O	0.50	15.0	3	SU
OSR-1	O	0.50	45.0	Static	SR
OSR-2	O	0.50	30.0	Static	SR
OSR-3	O	0.50	15.0	Static	SR
OSU-10	O	0.60	45.0	18	SU
OSU-11	O	0.60	30.0	18	SU
OSU-12	O	0.60	15.0	18	SU
OSU-13	O	0.60	45.0	9	SU
OSU-14	O	0.60	30.0	9	SU
OSU-15	O	0.60	15.0	9	SU
OSU-16	O	0.60	45.0	3	SU
OSU-17	O	0.60	30.0	3	SU
OSU-18	O	0.60	15.0	3	SU
OSR-4	O	0.60	45.0	Static	SR
OSR-5	O	0.60	3.00	Static	SR
OSR-6	O	0.60	15.0	Static	SR
ODR-2	O	0.50	30.0	9	DR
ODR-5	O	0.60	30.0	9	DR
ODR-7	O	0.50	30.0	3	DR
ODR-8	O	0.60	30.0	3	DR
ODR-9	O	0.50	30.0	18	DR
ODR-10	O	0.60	30.0	18	DR
ODR-11	O	0.50	30.0	Static	DR
ODR-12	O	0.60	30.0	Static	DR
VSU-1	V	0.53	15.0	18	SU
VSU-2	V	0.53	15.0	9	SU
VSU-3	V	0.53	15.0	3	SU
VSR-4	V	0.53	15.0	Static	SR
PW-1	O	0.50	45.0	9	SU
PW-2A	O	0.50	30.0	9	SU
PW-2B	O	0.50	30.0	9	SU
PW-3	O	0.50	15.0	9	SU
PW-4	O	0.60	45.0	9	SU
PW-5	O	0.60	30.0	9	SU
PW-6	O	0.60	15.0	9	SU

Chapter V

LABORATORY TEST RESULTS

It may be recalled from Chapter I of this study that the research was planned to contribute to the knowledge of the load deformation characteristics of cohesionless soils subjected to dynamic loading. In Chapter II, the results of Phase I, based upon theoretical evidence, established the significant difference between the dynamic loading as compared to normal or static tests for determining material characteristics. Prompted by these findings, the experimental program of Phase II was designed to explore this difference through study of three significant parameters; void ratio, confining pressure and loading rate. The results of each individual study are listed and discussed in the following sections.

Sections 5.2, 5.3 and 5.4 present test results of this research. Included among these results are those for saturated and dry sands, with measurements of the pore-water pressure under dynamic loading. Section 5.5 contains a summary of all the deformation effects which

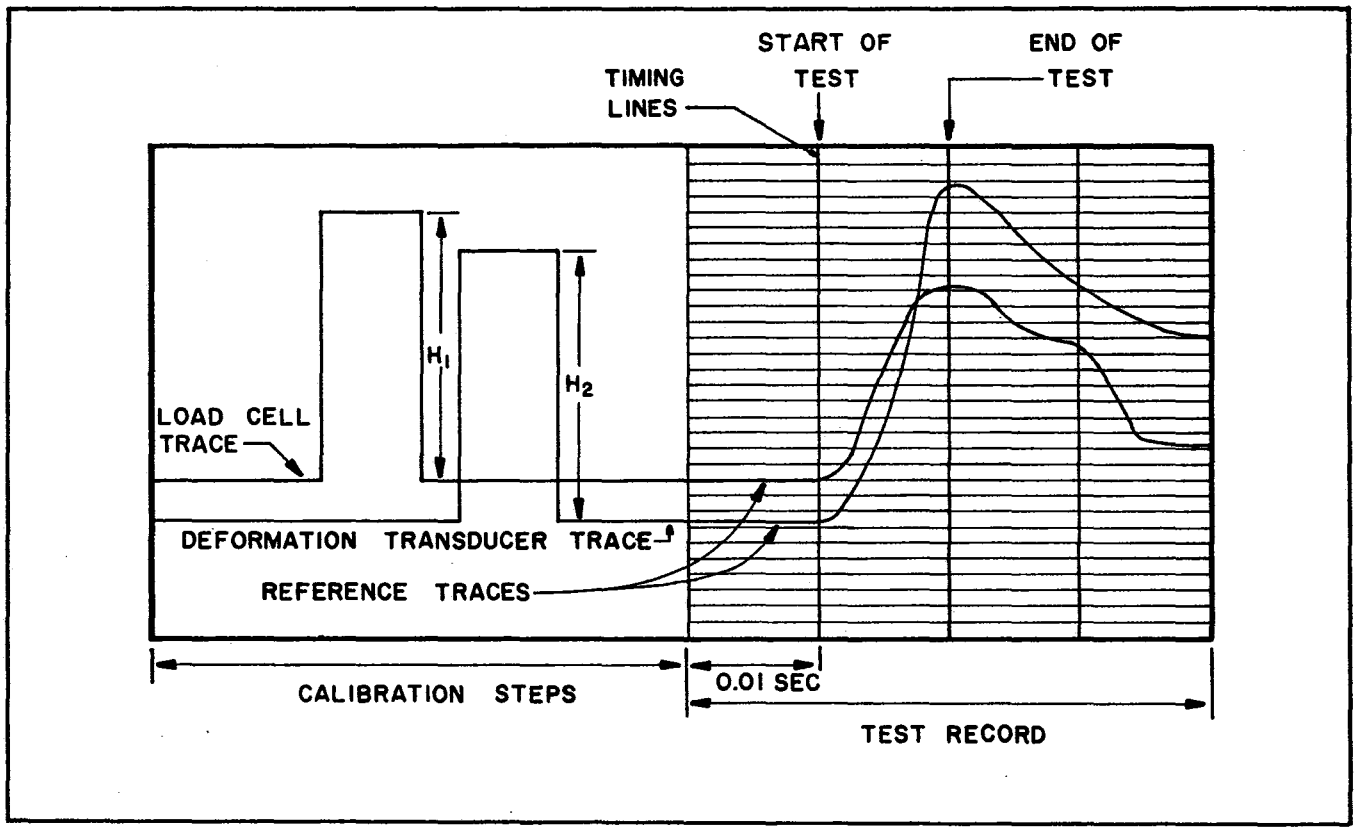

Figure 5-1. Oscillogram showing calibration steps and load and deformation traces.

have been obtained, including those obtained by earlier investigators.

5.1. Data Reduction

Load and Deformation. Fig. 5-1 illustrates an oscillogram showing the calibration steps and the record of the load and deformation during a test. The trace height, H, of the calibration step for the load cell is made by shunting a 60,000 ohm calibration resistor across one arm of the strain gaged load cell while the photographic paper of the oscillograph is slowly moving. This calibration resistor simulated 1720 lb. of load on the load cell. The trace height H_2 of the calibration step for the displacement transducer is made by sliding the shaft 0.934 in. back and forth while the photographic paper of oscillograph is slowly moving. Since the calibration steps are equivalent to a known load and a known deformation, the magnitudes of which are determined by the following formulas, respectively.

$$L = C_L \frac{h_1}{H_1} \qquad (5\text{-}1)$$

$$D = C_D \frac{h_2}{H_2} \qquad (5\text{-}2)$$

where

L = load in lb. at time t

D = deformation in in. at time t

C_L = load in lb. equivalent to the calibration step H_1

C_D = deformation in in. equivalent to the calibration step H_2

h_1, h_2 = heights in in. of the load cell and displacement transducer traces at time t, respectively

H_1, H_2 = heights in in. of the calibration steps for the load cell and displacement transducer, respectively

Pore-Water Pressure. The principle for evaluating the pore-water pressure from an oscillogram is similar to that of load calibration as described previously. The trace height H_3 of the calibration step for the pressure transducer is made by shunting a 60,000 ohm calibration resistor across one arm of the strain gage pressure transducer while the photographic paper of oscillograph is slowly moving. This calibration resistor simulated 32.0 psi of the pressure transducer. The calibration step is equivalent to a known pressure, the magnitude of which is determined by the following formula:

$$p = C_p \frac{h_3}{H_3} \qquad (5\text{-}3)$$

where

P = pressure in lb. per in.^{2} at time t

C_p = pressure in lb. per in.^{2} to the calibration step H_3

h_3 = height in in. of the pressure transducer at time t

H_3 = height in in. of the calibration step for pressure transducer

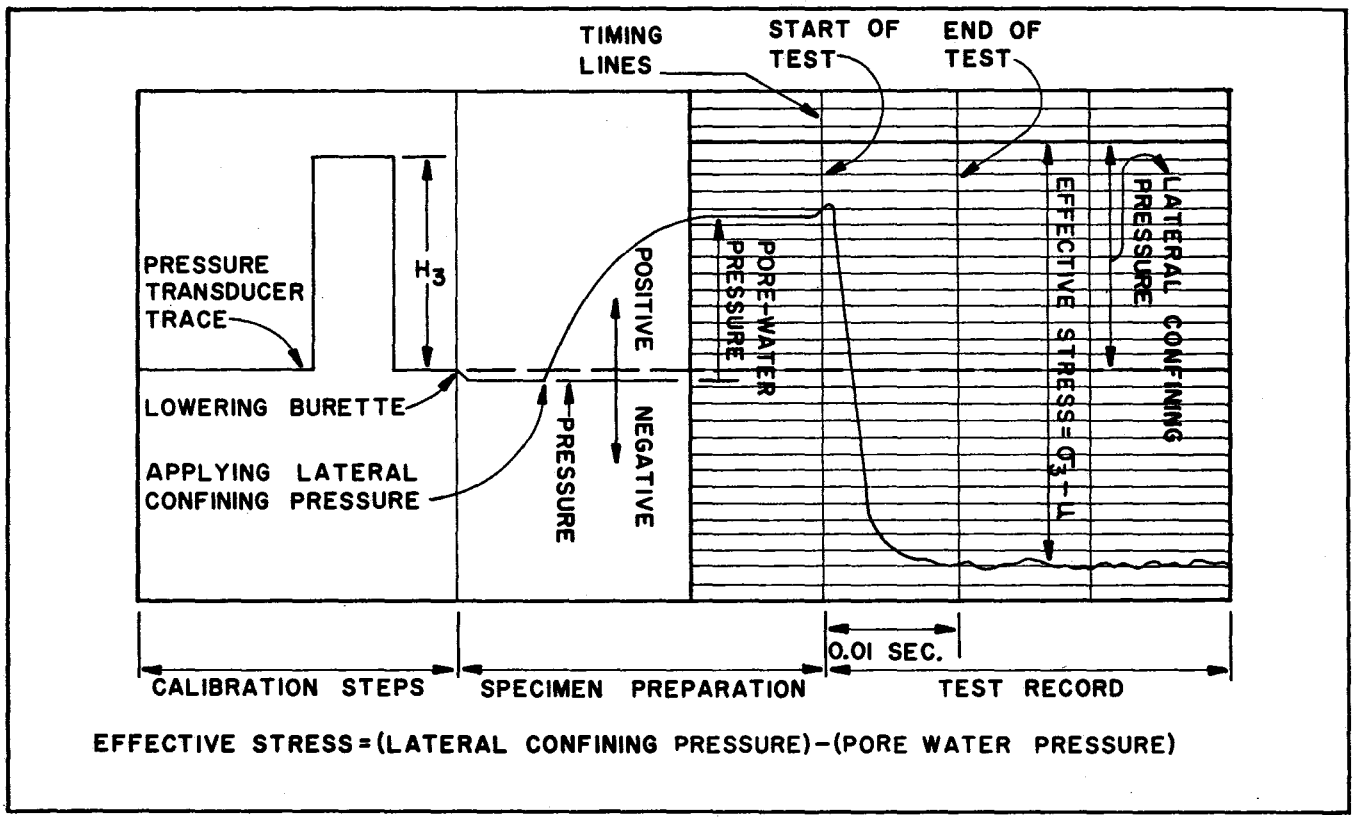

Figure 5-2. Oscillogram showing calibration steps and trace during preparation and testing of specimen for pore-water pressure.

An illustration for evaluating the pore pressure is given in Fig. 5-2.

5.2. Data Presentation

Theoretical considerations made it apparent that the most important factor affecting the results of the triaxial compression tests was the void ratio of the specimen. It was essential to know the initial void ratio accurately and for that void ratio to exist uniformly throughout the specimen if the results were to be reproducible. The skill and experience of the operator were major factors contributing to the uniformity of the results. A series of approximately 40 tests was performed in a preliminary stage of this research for the purposes of developing skill in preparation of test specimens and a more efficient operation of the equipment.

The results for various phases of this investigation are presented in the following sequences:

(a) Relationship between ultimate strength and rate of loading, and

(b) Dependence of ultimate strength on pore-water pressure.

5.3. Relationship of Ultimate Strength and Rate of Loading

This section presents a discussion on the rate of loading effect upon the strength of cohesionless soils. Loading rate effect means the tendency, if any, for the compressive strength of soil to increase or decrease with

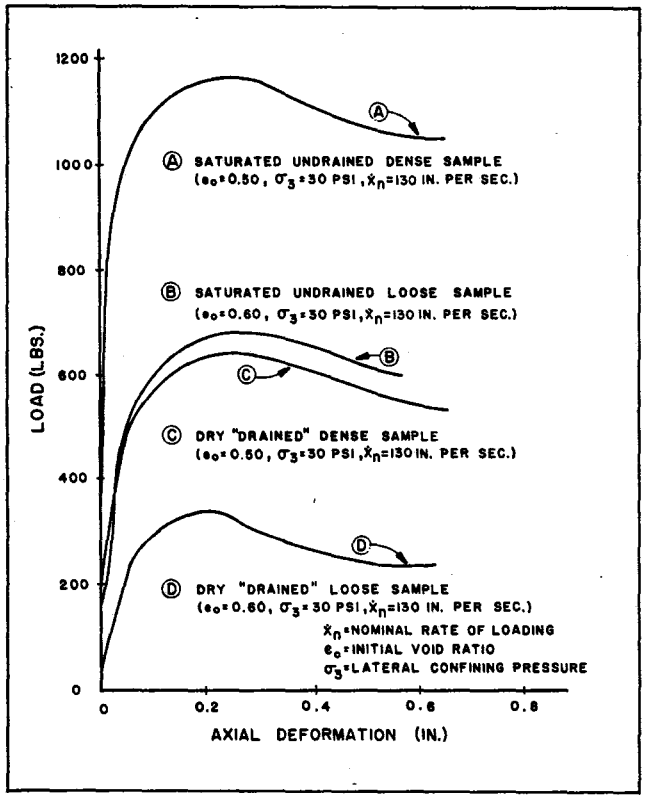

Figure 5-3. Typical load-deformation curves for Ottawa sand.

increasing rate of loading. Actually, the discussions will refer to all of the load-deformation curves for soils tested in axial compression, but the emphasis will be upon the development of a plastic flow failure (or ultimate strength) condition, which is important in the analysis of pile driving problems.

The results of these tests on Ottawa sand are divided into two main groups. The first group deals with dense saturated specimens and comparatively loose saturated specimens, and the second with dry specimens. Typical curves for each type of test are shown in Fig. 5-3. The reason for separating the tests by the states of specimens stem from the difference in behavior between the saturated specimens and dry specimens as regards the load-deformation curve and the pore-water pressure development.

5.3.1. Saturated Undrained Ottawa Sand. This section contains the description of a series of rapid dynamic triaxial compression tests performed upon saturated undrained samples of 20-30 Ottawa sand. The series of triaxial compression tests has been designated as OSU.

The samples of saturated Ottawa sand for this series of tests were prepared in the manner described in Section 4.2 of Chapter IV of this study. A total of 25 tests were performed in this series.

Saturated Dense Specimens $e_o = 0.50$ (Relative Density, $D_d = 68.5\%$).* Data showing the effect of the rate of loading on the ratio of ultimate dynamic to ultimate static strength are plotted in summary fashion in Fig. 5-4. The load-deformation curves from the individual tests are presented in Figs. 5-5 through 5-7. Additional tabulated data are incorporated in Appendix A.

For the tests, the curve of load versus deformation is essentially the same shape, regardless of the rate of loading. There was a pronounced "yield point" at approximately one per cent strain and then a flat curve portion that continued horizontally for approximately five per cent strain or until the end of the test.

As previously stated in Chapter II, the increase in strength of saturated undrained dense cohesionless soil specimens with increase in deformation-rate, can be attributed to the change in pore-water pressures. An attempt to develop some physical picture of the interrelationship of the various mechanism of pore-water pressure possibly contributing to the manifestations of

*The relative density, D_d, of the sample is defined by

$$D_d = \frac{e_{max} - e}{e_{max} - e_{min}}$$

For Ottawa sand 20-30, it was reported $e_{max} = 0.68$ and $e_{min} = 0.49$ (Ref. 38).

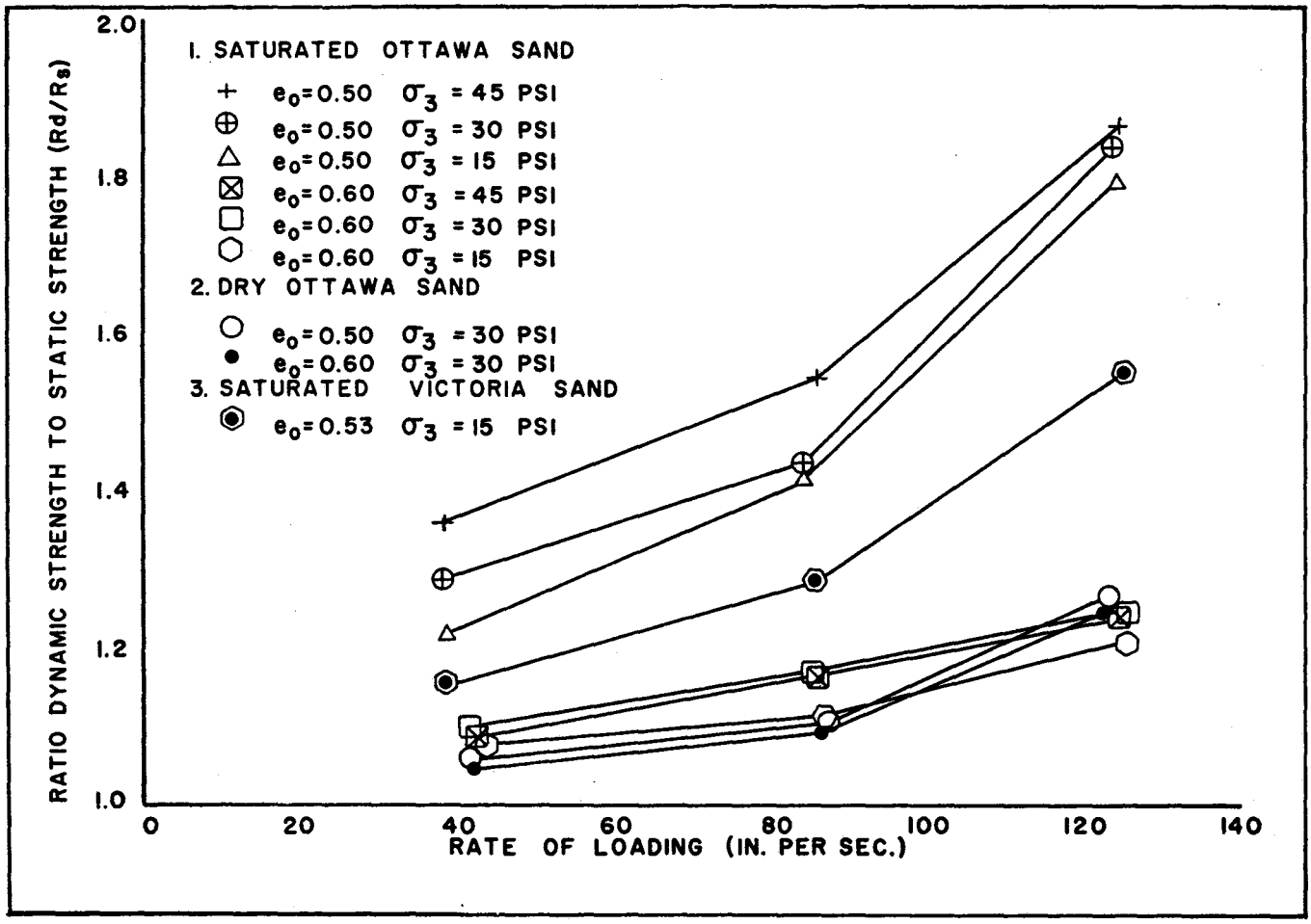

Figure 5-4. Increase in strength vs. rate of loading.

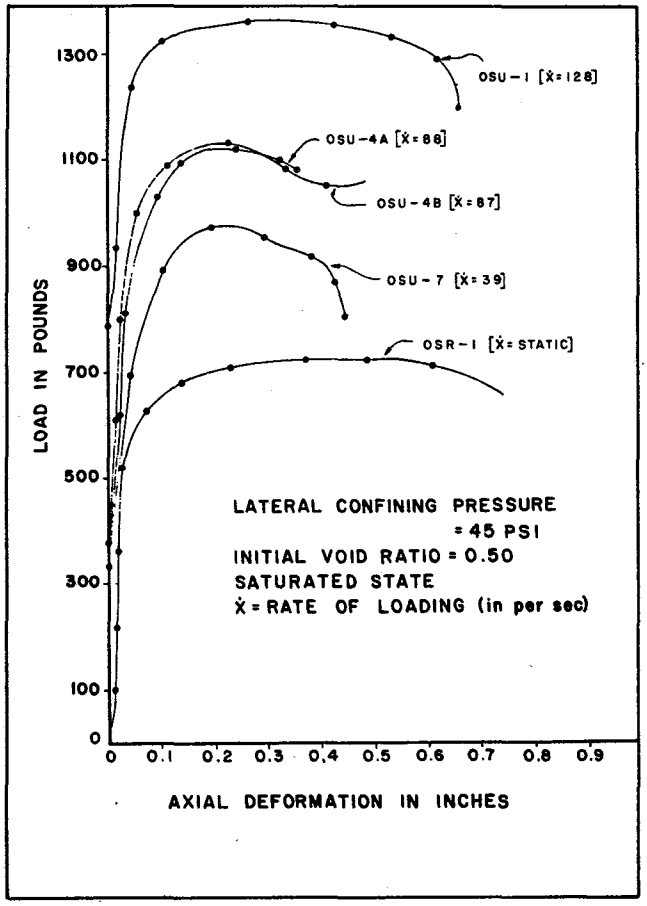

Figure 5-5. Load deformation curves for Ottawa sand.

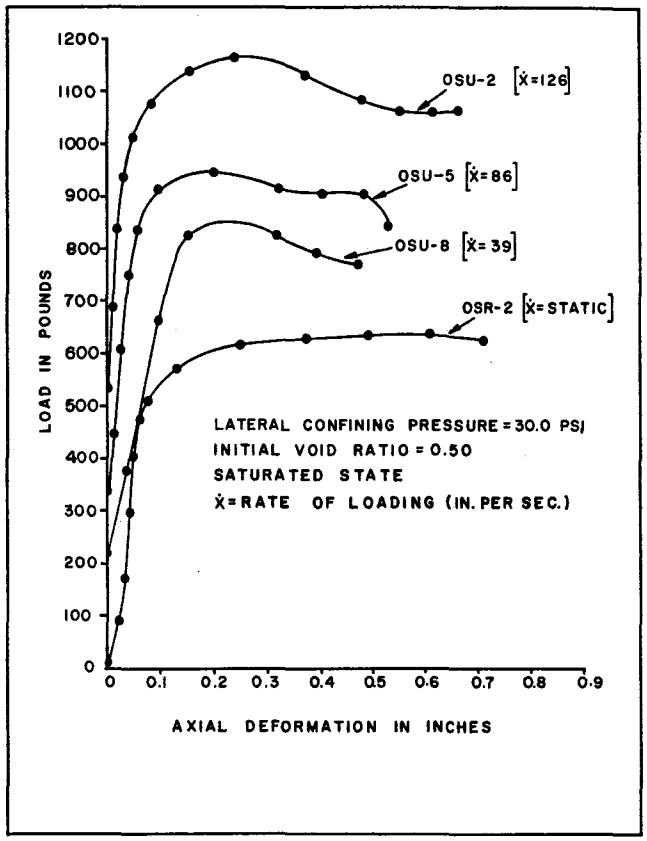

Figure 5-6. Load deformation curves for Ottawa sand.

saturated cohesionless soil will be undertaken in Section 5.4.

In looking at the effect of rate of loading on the strength of these specimens (Fig. 5-4) it can be seen that there is nearly 80% increase from static tests at a rapid rate of 120 in. per sec., and 30% increase from static tests at a rate of loading of 40 in. per sec. for the case of a lateral confining pressure of 45 lb. per in.^{2}

It is of interest to note that tests reported in this research are very similar to those reported by Seed and Lungren (Ref. 25) from their transient loading on Sacramento River sand and Monterey sand No. 5 dense specimens with lateral confining pressure at 30 lb. per in.^{2} Seed and Lungren reported that the dynamic strength increases approximately 15 to 20% at a rate of loading of 40 in. per sec. This range of values is very close to the range of values observed for Ottawa sand tested in this research. The results of this research indicate a 30% increase at 40 in. per sec. with a lateral confining pressure 30 lb. per in.^{2} The small difference between the two sets of results could be reasoned by various strength parameters of the sands involved.

It can also be seen from their data that there is no increase in strength due to rate effect on a loose saturated fine sand. This appears to point to the trend that the rate of loading effect decreases as the void ratio increases.

Tests of saturated cohesionless soil regarding the effect of rate of loading were also undertaken by Whit-

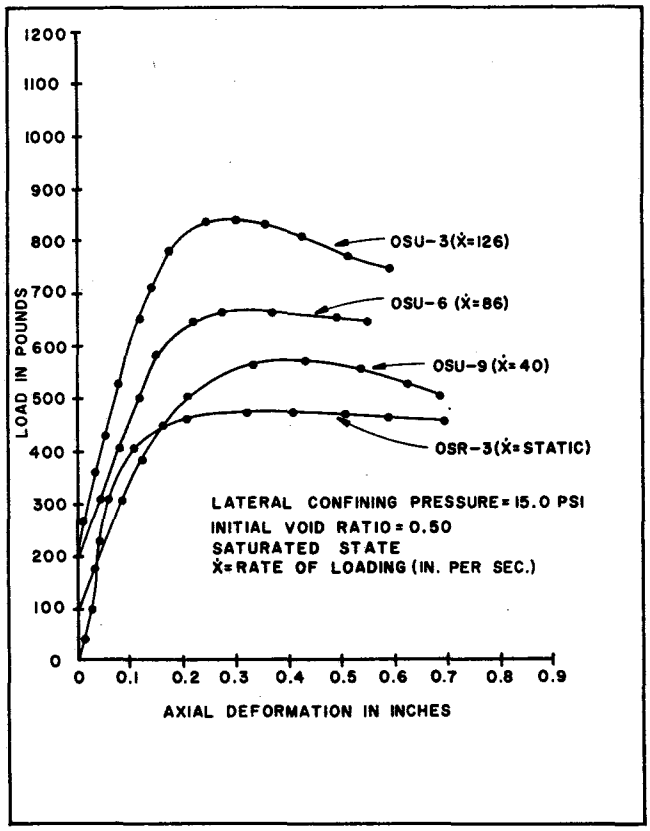

Figure 5-7. Load deformation curves for Ottawa sand.

man and his associates at Massachusetts Institute of Technology. It was reported (Ref. 38) that a total of 15 tests on Ottawa sand at a void ratio of 0.49 with pore pressure measurements, were run at three loading velocities: 0.012, 0.08, and 18 in. per sec. It was observed that the rate of loading had no noticeable effect upon the maximum axial stress. Whitman and Healy (Ref. 38) state:

> "The strain-rate had no noticeable effect upon the maximum axial stress, the friction angle, or the strain at maximum axial stress. The observed variation in peak friction angle was less than one degree. The pore-water cavitated at the same pressure regardless of strain-rate. Thus, the strain-rate behavior of this dense sand was very straight-forward.
>
> "The effects of membrane flexibility, of course, influenced these test results. However, had there been no membrane flexibility, the pore pressures would have decreased even more rapidly, and cavitation would have occurred at an even lower strain. The strain-rate effect results would have remained unchanged."

In essence, the observation made by Whitman and Healy was possibly correct for that particular range of loading rate. The difference, if any, it is felt, is due to the range in the rate of loading. The best solution of this dilemma appears to depend upon the nature of cohesionless material. This question will be discussed in Section 5.4.

Loose Specimens (e_o = 0.60, Relative Density, D_d = 42.0%.) In order to compare the dynamic effect with the dense specimens, Fig. 5-4 shows a summary of

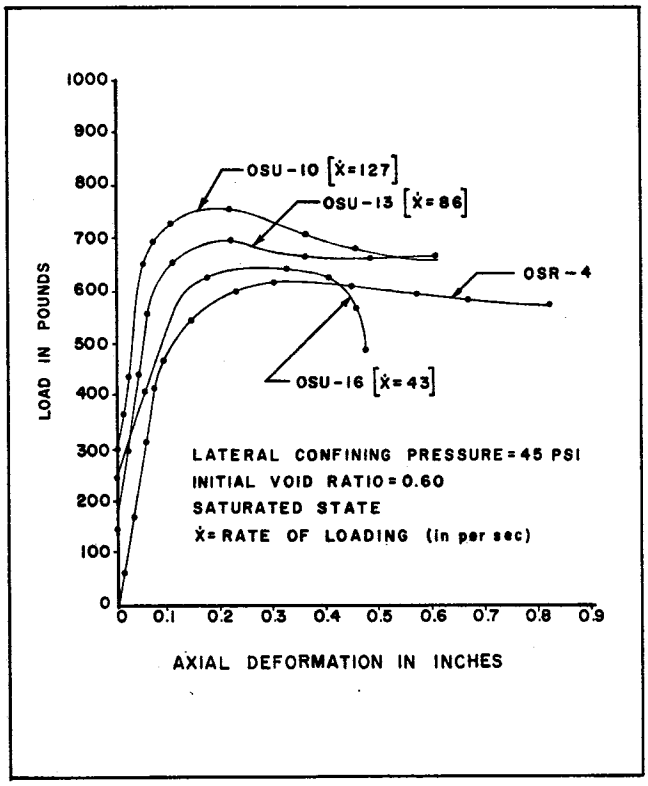

Figure 5-8. Load-deformation curves for Ottawa sand.

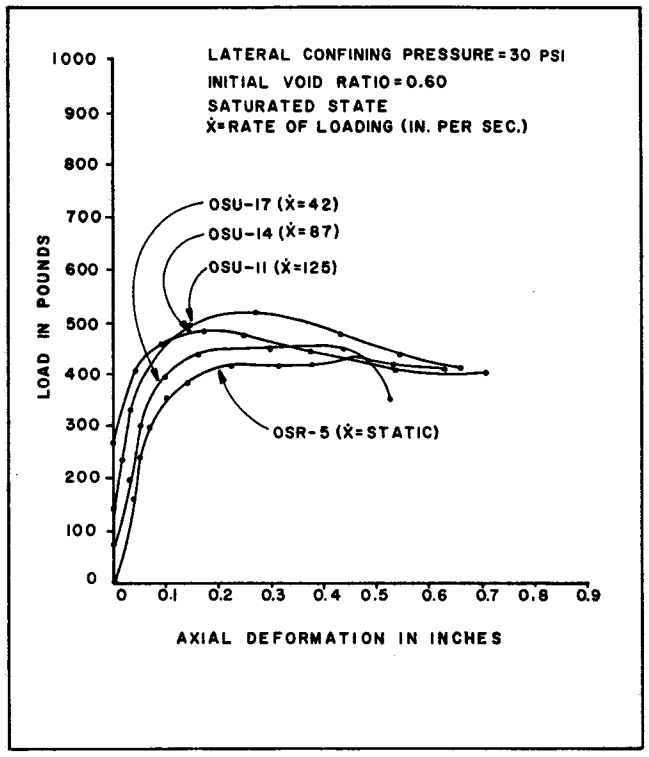

Figure 5-9. Load-deformation curves for Ottawa sand.

the effect of the rate of loading on the ratio of ultimate dynamic to ultimate static strength resulting from this series of tests. It can be noted that the specimens subjected to the higher rate of loading tended to dilate more than the slower rate of loading resulting in low pore-water pressures. The result of this tendency was to increase effective stress and, consequently, increase strength, also. For these tests, the curve of load versus deformation was essentially the same shape regardless of the rate of deformation. The load-deformation curves from the individual tests are presented in Figs. 5-8 through 5-10. Additional tabulated data are incorporated in Appendix A.

In general, the conclusions of this series are quite similar to the previous one, except the increase of strength subjected to dynamic loading is much milder. Similar conditions were observed by Seed and Lungren (Ref. 25).

5.3.2. Dry "Drained" Ottawa Sand. This section presents the results of a series of triaxial compression tests on dry Ottawa sand. The tests discussed were designed to provide some information concerning the effect of deformation-rate upon the behavior of dry sands on one hand, and of a supplementary nature to examine the behavior of pore-water pressure (Sec. 5.4). The nature of cohesionless material will be made clearer in the following discussion.

Data showing the effect of the rate of deformation on the ratio of ultimate dynamic to ultimate static compressive strength are plotted in summary fashion in Fig. 5-4. Load-deformation curves from the individual tests are presented in Fig. 5-11.

The results indicate that there is a slight increase in the shearing strength of dry sands as the rate of load-

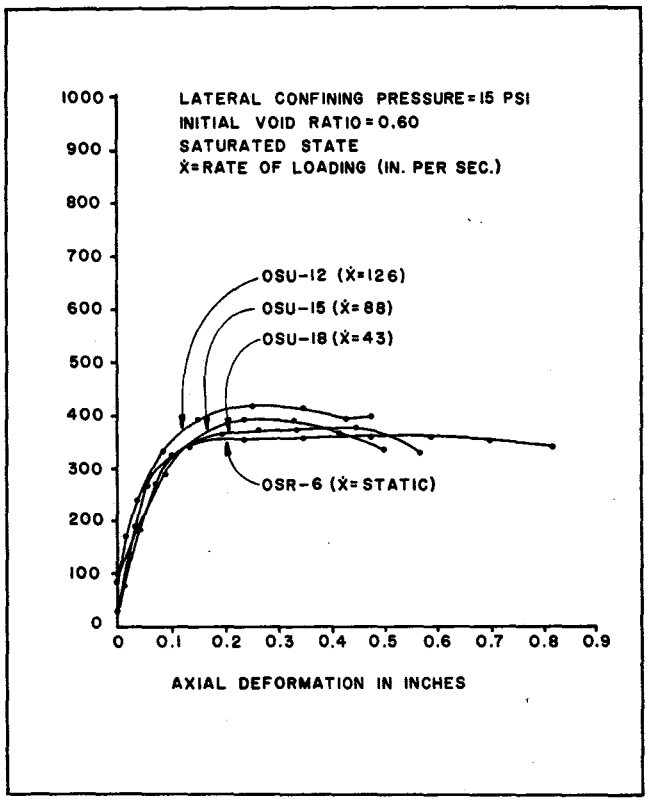

Figure 5-10. Load-deformation curves for Ottawa sand.

ing is increased from the static test. Data regarding the effect of rate of loading upon the shearing resistance of dry sands appears in reports of previous work (Ref. 4, 36).

The results of the studies regarding compressive strength as a function of rate of loading can be summarized as follows:

1. Tests by Casagrande and Shannon (Ref. 4) at Harvard University upon a clean, medium quartz sand suggested that the dynamic compressive strength of the sand might increase as much as 15 per cent greater than the static compressive strength. However, the range of data scatter roughly equaled the range of possible errors in such data.

2. Tests performed at Massachusetts Institute of Technology by Whitman and his associates (Ref. 36) indicate that the strength increases from a loading rate of 0.105 in. per sec. to a loading rate of 15 in. per sec. were 5 per cent at a vacuum of 12.8 lb. per in.,^{2} and 16 per cent at a lower vacuum. Standard Ottawa sand was used in these tests.

All of these studies indicate that there is a slight increase in the shearing strength of the dry sands as the loading rate is increased from that in the normal slow test to that in a rapid dynamic test. In view of the observed amounts of normal static test and rapid dynamic tests, the magnitude of the dynamic effect might be 10 to 15 per cent increase. From the practical point of view, the dynamic effect is so small as to be of no practical importance. Nevertheless, the characteristics of dry sands are of considerable interest in order to understand the nature of the load-deformation mechanism within granular masses.

5.3.3. Saturated Undrained Victoria Sand. These tests on Victoria sand like those discussed in the preceding sections were undertaken to study the dynamic effect characteristics. Four specimens were tested at four different loading rates, i.e., 130 in. per sec., 80 in. per sec., 40 in. per sec., and static rate, with a lateral confining pressure of 15.0 lb. per in.,^{2} and an initial void ratio of 0.53. The same mold and techniques were employed in the Ottawa sand (see Section 4.2, Chapter IV).

The tests results of load-deformation curves are shown in Fig. 5-12. Detailed tabulated data are also incorporated in Appendix A in which VSU denotes the saturated undrained triaxial compression test on Victoria sand.

The results of this series on the fine sand show essentially the same phenomena as occurred in the tests on Ottawa sand. It is noted a pronounced "yield point" at approximately one per cent strain and then a flat curve portion that continued for approximately four to five per cent strain or until the end of the test. It is of interest to note the general trend for the strength to increase with the rate of loading. Reference to the plotted data also shows that this trend is well defined and the implication is that Victoria sand exhibits moderate dynamic effect. The ratio of ultimate dynamic strength to ultimate static strength has been plotted against the loading rate in Fig. 5-4.

As was stated at the outset of Chapter IV, the results of these four tests were of an appurtenant nature and permitted only conclusions on dynamic effect to be drawn. It is felt that an independent study on this soil

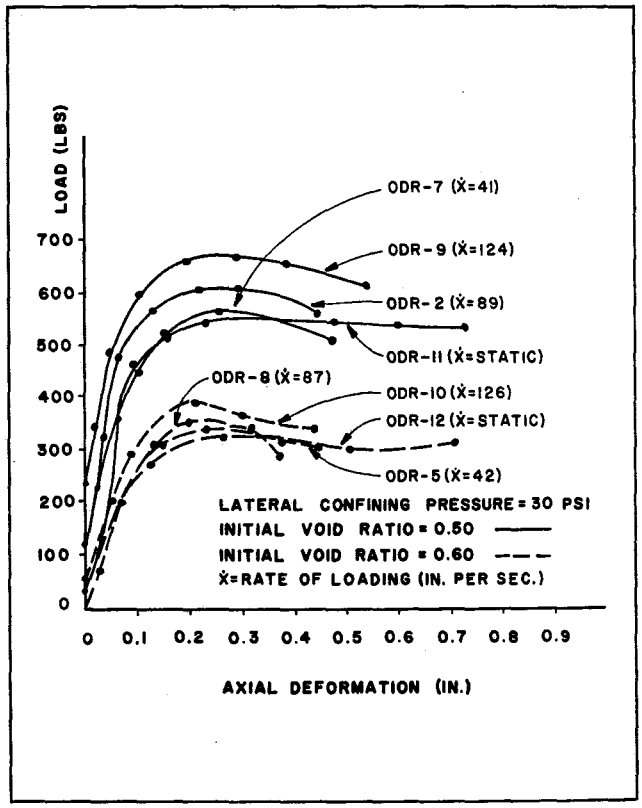

Figure 5-11. Load-deformation curve for dry Ottawa sand.

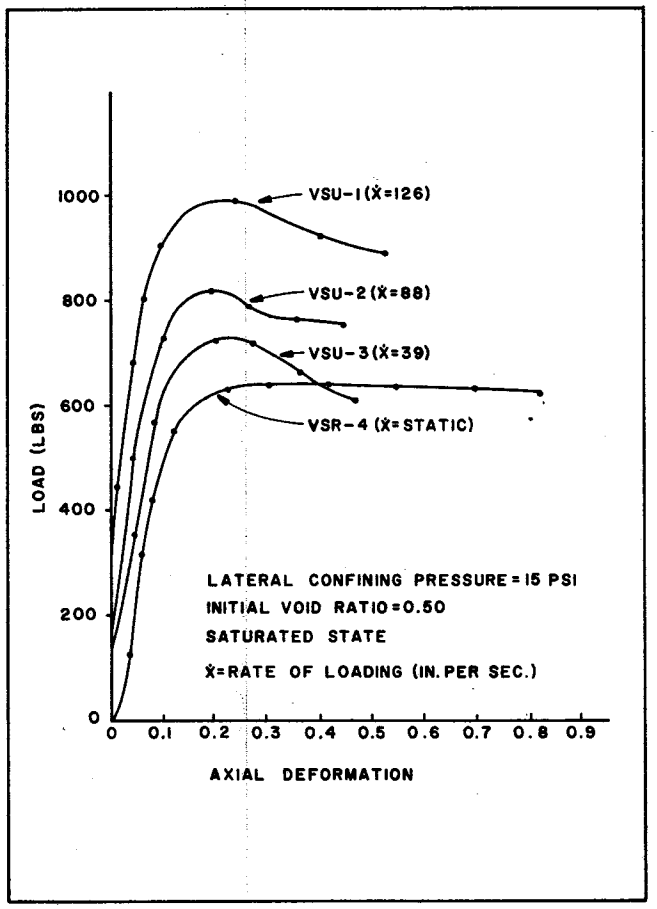

Figure 5-12. Load-deformation curves for Victoria sand.

would provide new understanding of the behavior of a predominantly fine grained cohesionless soil.

5.4. Dependence of Ultimate Strength on Pore-Water Pressure

It was recognized at the beginning of this research program that the pore-water pressure which occurs within the soil samples under dynamic load might prove to be one of the important factors that influence the dynamic load-deformation characteristics of a cohesionless soil. A brief explanation of pore-water pressure behavior on undrained triaxial tests subjected to a "static" load has been given in Section 2.3, Chapter II. The implication of this principle is that volume change due to the deformation in the cohesionless soil produces a reduction in pore-water pressure, μ. Therefore, until some knowledge is gained concerning the behavior and magnitude of pore-water pressures, all of the available data regarding the effect of the rate of deformation upon shear strength cannot be applied with any great confidence to field problems.

A series of pore pressure measurements has been designated as PW tests. A total of six tests was performed in this series. The test results are divided into two groups. The first group deals with initial void ratio, $e_o = 0.50$, and the second with initial void ratio $e_o = 0.60$. Three different lateral confining pressures were employed (15, 30 and 45 lb. per sq. in.). Loading at a rate of 80 in. per sec. was accomplished using the dynamic load test apparatus described in Section 3.1.2, Chapter III. Details for measuring pore pressure are also explained in Section 4.4, Chapter IV.

The pore-water pressures recorded from the series of PW-triaxial compression tests subjected to rapid dynamic load as a function of lateral confining pressure have been reduced and are given in Table 5-1. Also, the effective stresses have been determined and are recorded in Table 5-1 and plotted in Figure 5-13. The fundamental characteristics underlying the pore-water pressure on a dilatant soil is that the pore-water pressure normally undergoes a slight increase at small strains and then decreases as the structure tends to dilate. This is shown in Figure 5-2. In Figure 5-13, the initial effective stress and the effective stress at failure have been plotted against lateral confining pressure.

The discussion that follows is an attempt to develop some picture of the inter-relation between ultimate strength and pore-water pressure in a sample subjected to rapid dynamic load.

The drop in pore-water pressure under certain conditions may be sufficient to produce negative values (see Fig. 5-14). The correlation of the negative pore-water pressure and the fundamental shear strength properties has been pointed out by Seed and Lungren (Ref. 25). They state:

> "When a dense saturated sand is deformed, the void ratio is increased, and if there is no time for seepage into the sand, the water can no longer fill the voids. As a result the pore-water is pulled in tension (sometimes called a negative pore-water pressure), thereby increasing the pressure between the grains and causing a temporary increase in strength."

TABLE 5-1. CHARACTERISTICS OF EFFECTIVE STRESS UNDER DYNAMIC LOADING*

Test No.	Confining Pressure (psi)	Initial Void Ratio (e)	Initial Pore Pressure (psi)	Initial Effective Stress (psi)	Reduction in Pore Pressure (psi)	Effective Stress at Failure (psi)
PW-1	45	0.50	38.3	6.7	53.0	59.7
PW-2A	30	0.50	22.5	7.5	37.2	44.7
PW-3	15	0.50	8.3	6.7	13.0	19.7
PW-4	45	0.60	41.5	3.5	26.2	29.7
PW-5	30	0.60	27.7	3.5	26.2	29.7
PW-6	15	0.60	12.8	2.3	20.5	22.8

*NOTE—Loading rate for all PW tests was nominally 80 in. per sec.

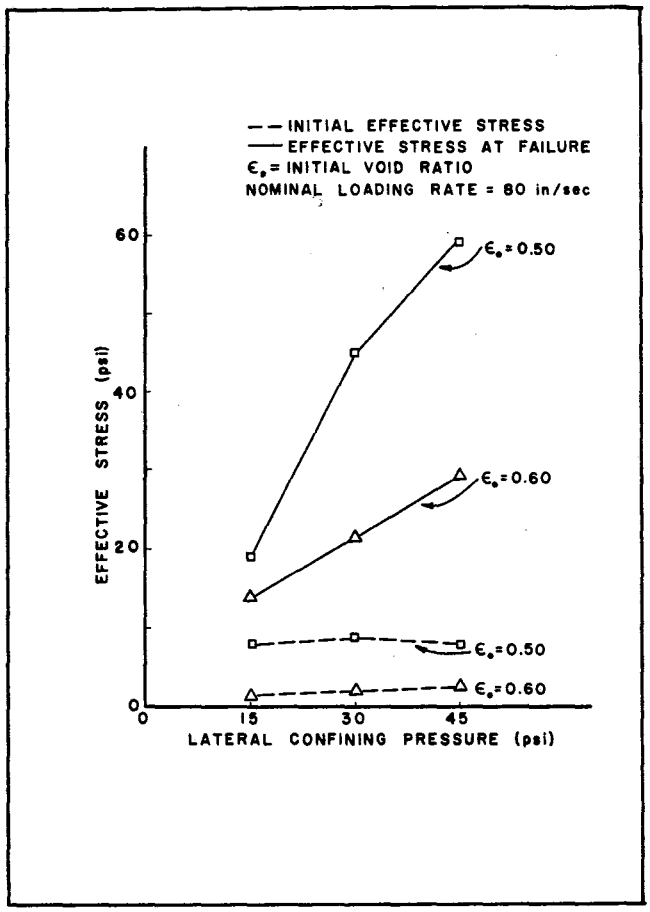

Figure 5-13. Effective stress measurements.

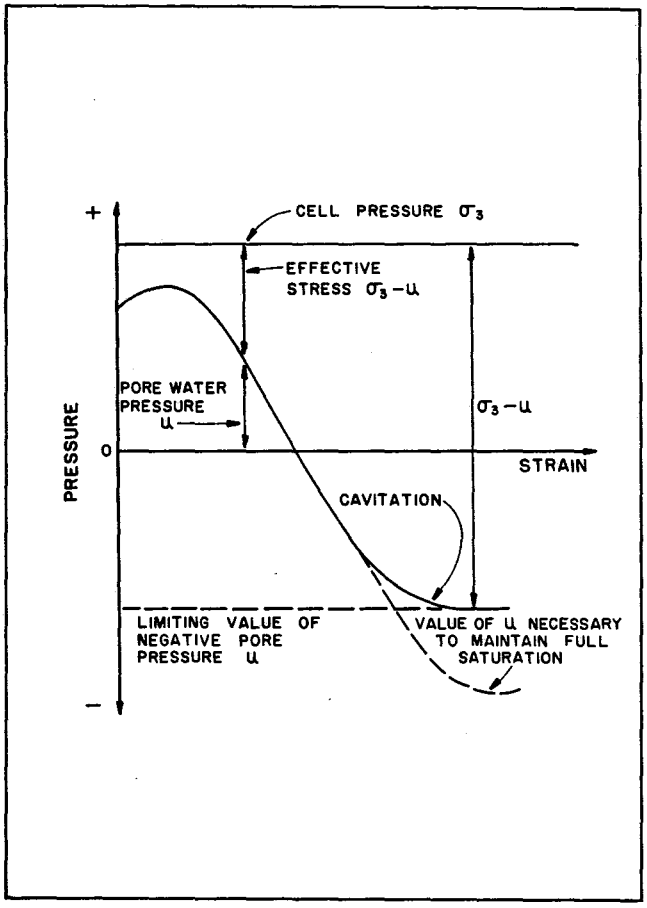

Figure 5-14. Pore-pressure changes in dilating sample (after Bishop and Eldin, Ref. 1).

The significance of the above statement can be expressed by the Coulomb-Hvorslev equation (Eq. 2-3). Thus, one can see that

$$\tau = [\sigma - (-\mu)] \tan \phi$$
$$\tau = [\sigma + \mu] \tan \phi \qquad (5\text{-}4)$$

It should be pointed out that 14.7 psia is the maximum value of negative pore pressure that can be obtained. However, in addition to pore-water pressure changes, the rate of loading must be considered.

Seed and Lungren state:

> "The strength of a dense saturated sand under transient loading conditions is greater than for normal rates of loading due to (1) the effects of dilatancy combined with lack of drainage, and (2) the effects of the rate of deformation."

In discussing the first factor, it is believed by this investigator that the changes in pore-water pressure are due to the inability of water to drain freely during very rapid tests. It has been indicated in static tests that the sand tends to dilate in a very dense specimen at which cavitation or vaporization occurs (see Fig. 5-14). In order to cavitate, nucleation must occur, and a site for nucleation must be found. The search for a nucleation site is time dependent, and water could be expected to obtain an absolute tension in a rapidly loaded specimen.

It was indicated in this investigation that for a given void ratio, the effective stress increases as the confining pressure increases at the same rate of loading (see Fig. 5-13). It is important to remember that these few tests on pore-water pressure measurement were of a preliminary nature, and hence the above discussion represents more the manner in which such analyses may be made rather than indicating positive conclusions regarding this saturated cohesionless soil. This may be an interesting area for further investigation.

Chapter VI

RHEOLOGICAL MODEL STUDIES

6.1. Rheological Damping Properties of Cohesionless Soils

In order to be able to relate the time effects observed in these tests with the dynamic effect and other phenomena, and in order to utilize these data in the study of pile-driving analysis involved in a pile-soil system, it is desirable to have expressions for the behavior of the soil in the form of mathematical equation. This is a similar situation as in continuum mechanics,

where the term "constitutive equation" is being used to describe the properties of material, or structural system (Ref. 35). If the constitutive equation is to be a general one, then it should include all sensitive and conceivable details of all conceivable inputs and which are able to predict all details of the output. Such equations, in general, are extremely complicated. They would be so cumbersome mathematically as to be unsolvable. Thus, simplified, idealized, or limited form of constitutive equations are generally required. For the present purposes, we are concerned primarily with the load-deformation-time properties of cohesionless soils. As a result, the damping properties study is undertaken according to the phenomenological approach.

In undertaking this work, it is convenient first to define a rheological model which will simulate to a reasonable degree the behavior of the material investigated. Secondly, it is desired to derive the "load-deformation-time" equation relating to force-deformation-time derivatives of these quantities.

It is necessary to point out that the task of determining a rheological model to simulate the complex behavior of soil is generally far from simple. An example of such a task is illustrated by Klansner (Ref. 19).

The proposed model is shown in Fig. 6-1. The two elements included in the model are all necessary to meet the basic requirements described by Smith (Ref. 28).

> "The ground compresses elastically for a certain distance and then fails plastically with constant or 'ultimate' resistance Ru. This concept is illustrated in Fig. 4."

(Fig. 6-2 of this report.)

Applying this notion to the present problem, we can arrive at a rheological model similar to that which was described by Lord Kelvin. Diagrammatically it can be represented by a spring (or Hookean solid) coupled with a dashpot (or Newtonian Fluid) as shown in Fig. 6-1, except its notations, which may be called a Kelvin-body, or Kelvin-Voigt body.* The mathematical relation for the Kelvin-body is

$$\sigma_o = \mu\epsilon + \eta\dot{\epsilon} \qquad (6\text{-}1)^{**}$$

where

σ_o = applied stress

μ = modulus of spring

ϵ = strain

η = viscosity of the dashpot

$\dot{\epsilon}$ = differentiation of strain with respect to time

Smith made use of the rate-effect for his simulation of the pile-soil system (Fig. 6-2). However, in order to apply Eq. (6-1) for the present problem, one must evaluate the modulus of spring as well as the viscosity of the dashpot. This is a cumbersome procedure, as a result, a modified form was given by Smith (Ref. 28):

*The mathematical relation for this rheological model was derived by Voigt (1890), but the idea was originally due to Lord Kelvin (1878).

**See Appendix D.

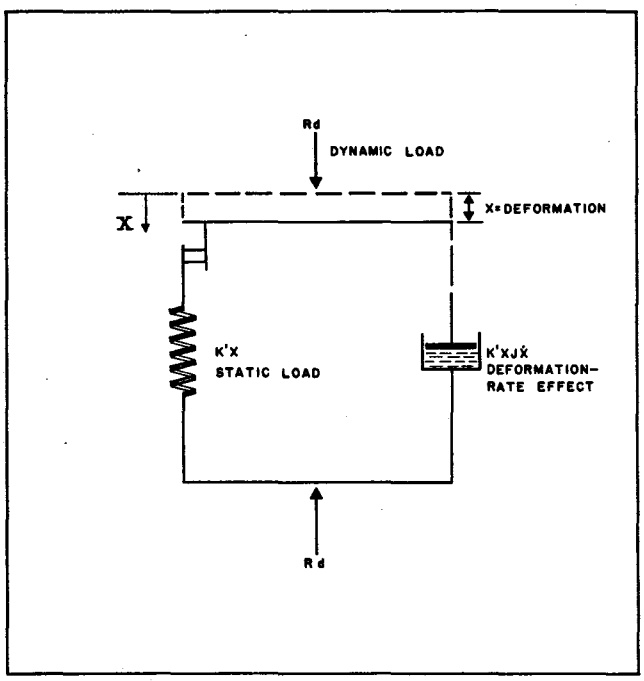

Figure 6-1. Smith's model for describing dynamic load-deformation properties of soil.

$$R(m,t) = [D(m,t) - D'(m,t)]\, K'(m)\, [1 + J(m)\, V(m, t-1)] \qquad (6\text{-}2)^{*}$$

or, more conveniently,

$$Rd = K'x\,(1 + J\dot{x}) \quad \text{for} \quad 0 \leq x \leq Q \qquad (6\text{-}3)$$

where

Rd = R(m,t) = dynamic resistance of soil (lb.)

K′ = K′(m) = spring constant**

x = [D(m,t) − D′(m,t)] = deformation (in.)

J = J(m) = rheological damping factor

$\dot{x}$ = V(m,t−1) = differentiation of deformation with respect to time; in the case of pile-driving, $\dot{x}$ is the velocity of pile point

Q = Quake

If the rate of deformation approaches zero, Eq. (6-3) can be written approximately as follows:

$$R_s = K'\,x \qquad (6\text{-}4)$$

Now, the rheological damping factor can be readily evaluated as follows:

$$J = \left(\frac{R_d}{R_s} - 1\right)\frac{1}{\dot{x}} \qquad (6\text{-}5)$$

The principal information obtained from the tests upon Ottawa sand and Victoria fine sand has been

*See Eq. (1-6), Chapter I. of this report.

**For spring constant, see Table A-35, Appendix A. where R_s = static resistance of soil (lb.).

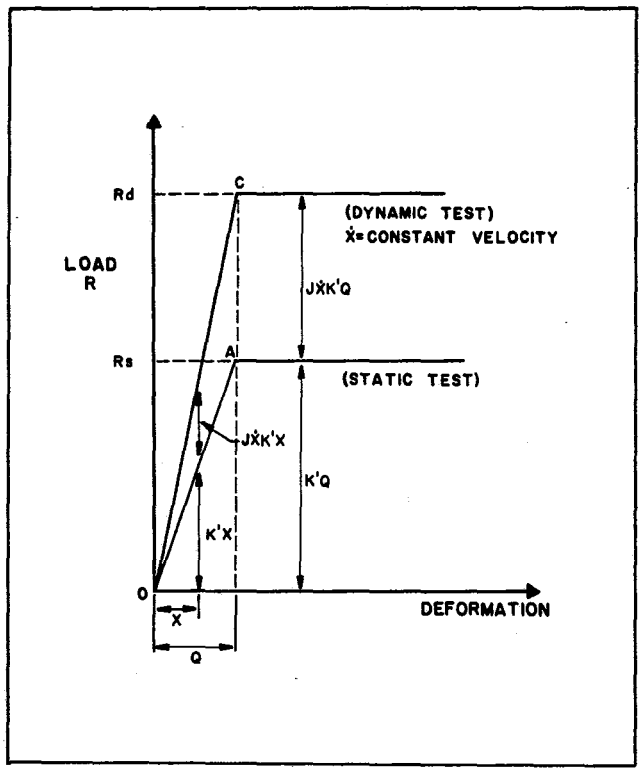

Figure 6-2. Idealized dynamic and static load-deformation curves..

summarized in Table 6-1. It is worthwhile noting that the damping factor is dependent upon two main factors: (1) initial void ratio, (see Fig. 6-3), and (2) state of specimen (saturated or dry) (see Table 6-1). It appears that a viscous mechanism is responsible for the damping. Presumably, this damping results from flow of water relative to soil particles. The use of the rheological model to simulate dynamic behavior of soil is discussed at length in the following paragraphs of this chapter.

6.2. Discussion of Rheological Models

Rheology is the science of deformation and flow, or precisely, as defined by Reiner (Ref. 20). Rheology as the physics of deformation, deals with the coordination of the forces acting upon material body and the deformation produced. A body is said to be deformed when application of a force system alters the shape or size of the body. A body is said to flow if its degree of deformation changes continually with time.

The goal of rheology is depiction of the force system necessary to cause a given deformation or flow in a body, or conversely depiction of the deformation of flow resulting from the application of a given force system to a body.

There are three different basic bodies defining the fundamental rheological properties. They are: (1) Hookean body, (2) Newtonian liquid, and (3) St. Venant body. The Hookean body, which is a perfectly elastic solid, is treated in the classical theory of elasticity. The Newtonian liquid, which is a "simple" viscous liquid, is treated in classical hydrodynamics. The St. Venant body is a solid which possesses a yield point below which it is strained elastically, but above which it flows plastically at constant stress, and which is the subject of ideal plasticity. Consequently, complex properties result from combinations of the fundamental properties, such as represented by complex models. Theoretically speaking, the combination of these complex models is unlimited, but in practice, limited in number. (Special designations have been coined for some of them, namely viscoelasticity, delayed elasticity, anelasticity and dynamical plasticity.)

Essential rheological properties can be systematically expressed in a hierarchy of ideal bodies. In this, the three fundamental bodies can be designated by the following symbols: H = Hookean solid, N = Newtonian liquid, and St. V. = St. Venant bodies. These three elements can be coupled either parallel (1) or in series (—). Therefore, the complex rheological model can be expressed in a "shorthand" form. Fig. 6-4 shows a "tree" of rheological bodies which have been postulated either on theoretical grounds or from empirical considerations. Other combinations are possible and

TABLE 6-1. SUMMARY OF RHEOLOGICAL DAMPING COEFFICIENT (J)

Test No.	σ_3 Lateral Confining Pressure psi	$\dot{X}_n$ Nominal Rate of Loading (in. per sec.)	Rheological Damping Coefficient
GROUP I. OTTAWA SAND; SATURATED STATE; INITIAL VOID RATIO = 0.50			
OSU-1	45	130	0.114
OSU-2	30	90	0.080
OSU-3	15	40	0.070
OSU-4A	45	130	0.076
OSU-5	30	90	0.062
OSU-6	15	40	0.059
OSU-7	45	130	0.082
OSU-8	30	90	0.080
OSU-9	15	40	0.077
GROUP II. OTTAWA SAND; SATURATED STATE; INITIAL VOID RATIO = 0.60			
OSU-10	45	130	0.034
OSU-11	30	90	0.033
OSU-12	15	40	0.031
OSU-13	45	130	0.018
OSU-14	30	90	0.018
OSU-15	15	40	0.020
OSU-16	45	130	0.012
OSU-17	30	90	0.012
OSU-18	15	40	0.020
GROUP III. OTTAWA SAND; DRY STATE; INITIAL VOID RATIO = 0.50			
ODR-9	30	130	0.028
ODR-2	30	90	0.011
ODR-7	30	40	0.002
GROUP IV. OTTAWA SAND; DRY STATE; INITIAL VOID RATIO = 0.60			
ODR-10	30	130	0.030
ODR-8	30	90	0.008
ODR-5	30	40	0.002
GROUP V. VICTORIA SAND; SATURATED STATE; INITIAL VOID RATIO = 0.50			
VSU-1	15.0	130	0.058
VSU-2	15.0	90	0.021
VSU-3	15.0	40	0.005

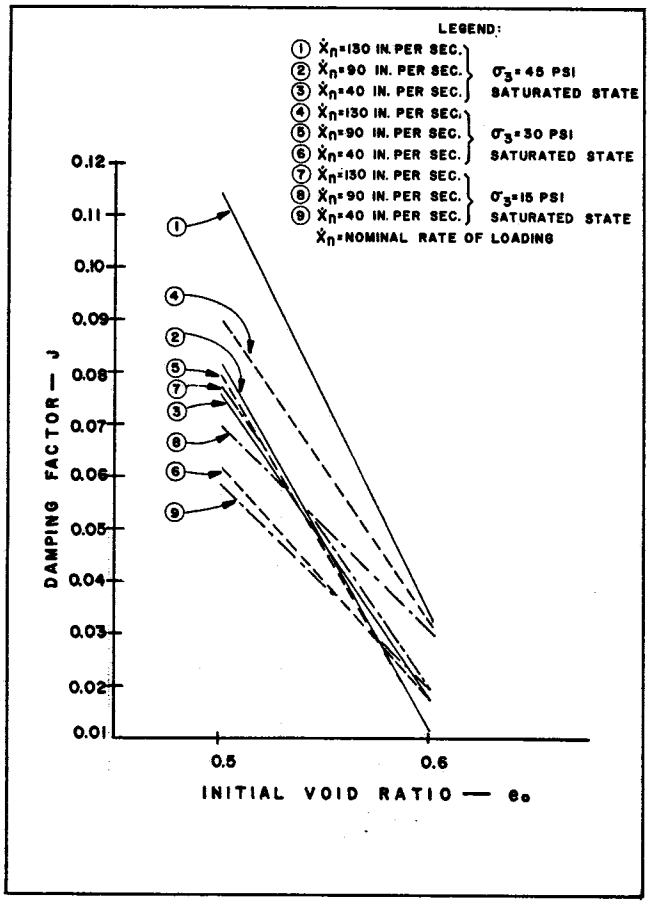

Figure 6-3. Rheological damping coefficients for Ottawa sand.

may arise, in order to describe the rheological behavior of materials not investigated so far. However, it can be seen that every real material possesses all rheological properties, albeit in every degree.*

It is clear that the theories of soil mechanics, fluid mechanics, elasticity, plasticity, strength of material and many fields of engineering, therefore, have their foundations, at least in part, in the science of rheology. The method of each of these theories is to combine a rheological result with the requirements of mechanics so as to obtain interesting and useful results about the class of materials of primary interest to the discipline. Hence, it is worthwhile to mention that rheology is not merely a grouping of mathematical expressions, or a playground for the theorists, but can throw light on the mechanical problems of immediate practical interest.

In order to be able to relate the time effects observed in tests of soil specimens, for example, for the study of deformation-rate effect, and in order to utilize the data in the study of pile-soil system and other phenomena, it is desirable to express the behavior of the soil media in the form of mathematical equations.

Moreover, rheological models are only utilized to represent physical properties of continua. The macroscopic point of view is applied. It should be kept in mind that the models do not describe the true or microscopic nature of substances. The most that can be expected of the models is to assist a mathematical expression in representation of physical phenomena.

*Reiner claimed this is the first axiom in rheology.

In soil mechanics, rheological models have been used by many investigators. In his theory of consolidation, for example, Terzaghi (Ref. 31) described the process of consolidation of a piece of clay by means of the Kelvin model. Improvement of the Terzaghi theory was made by Taylor et al. (Ref. 30), who proposed different models.

The present discussion does not cover the complete domain of rheology. However, one might conclude that the concept of rheological modeling is a pseudotechnique that adds versatility to continuum mechanics. It should be pointed out as more knowledge is gained about the true behavior of the material, rheological models could conceivably translate this information into a more exact language of continuum. As Reiner states (Ref. 20):

> "What we have described are not properties of real material. They are properties of abstract concepts which we have found ourselves in order to describe the behavior of real materials.
>
> "In reality, every material possesses all rheological properties, although in varying degrees."

6.3. *Rheological Model to Represent the Dynamic Response in Cohesionless Soil*

Let us begin by describing the model which was selected and then discuss the degree to which its be-

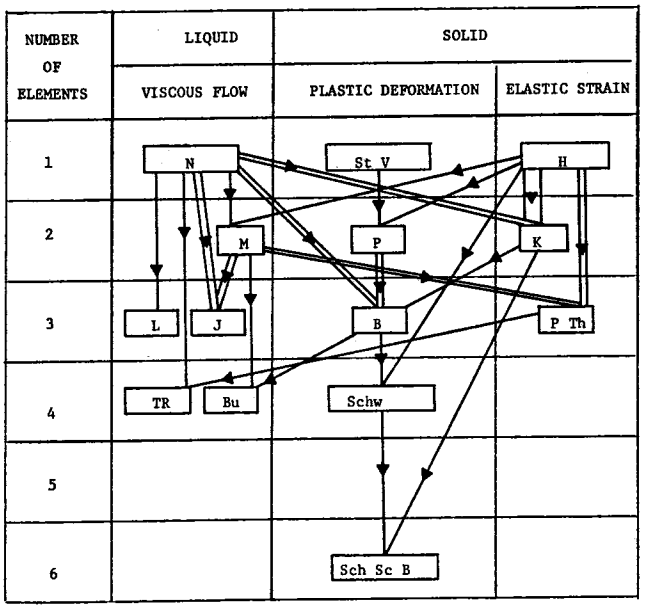

Figure 6-4. Tree of rheological bodies (after Reiner, Ref. 20).

havior is similar to that of sand. The model is shown in Fig. 6-1. The two elements included in the model are all necessary to meet the two basic requirements:

1. Under an instantaneously applied load (dynamic load), the model should undergo an instantaneous deformation and approach a limiting load value.

2. The greater the rate of loading, the steeper the curve in the load-deformation diagram.

It is necessary to point out that two main objectives may arise in this model. First, the response of such a model is linear. It is known that the load-deformation behavior of sand departs from a linear condition once a certain level of stress has been reached. This objection can to a large extent be overcome by the use of a spring with non-linear characteristics. The second objection is that the response of the model is reversible, whereas it is well known that the strain response of soil is definitely not reversible. It is possible to improve the similitude of action of the model in these two respects, but with such alteration, the complexity of the attendant, mathematics increases rapidly.

For use in this study, the two-element model has been adopted as a compromise between the conflicting requirements of realism and simplicity. Another significant factor influencing the choice of this model was the availability of solutions to the pile-driving analysis for material obeying the proposed solution.

The results presented in the previous chapter on the dynamic tests indicate that the ultimate strength of a cohesionless soil under rapid dynamic loadings is considerably different than under static loading. These studies indicated important dynamic effect. In addition, the ratio of static to dynamic state of stress has been shown to be very important (Fig. 5-4).

Therefore, it is reasonable to consider that the material constants required to describe the deformation characteristics of the soil are implicit in a characteristic soil strength parameter and the rheological viscosity. The characteristic soil strength parameter to be used is the spring constant of the soil (K). The rheological viscosity (J) controls the rate at which the deformation takes place. It is believed by the present investigator that the rheological viscosity of a saturated cohesionless soil is solely affected by pore-water pressure.

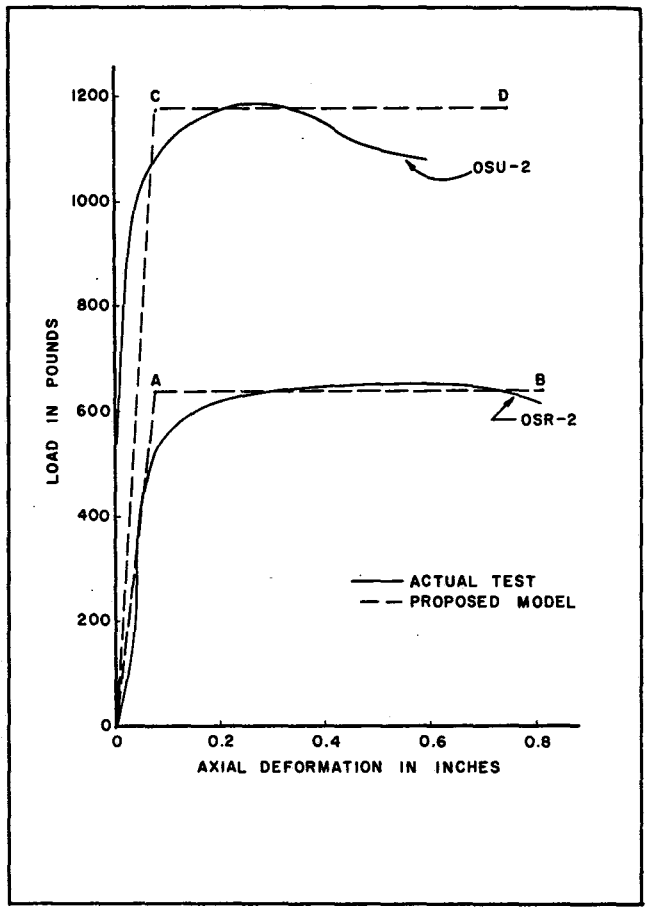

Figure 6-5. Typical test results vs. proposed rheological model.

Fig. 6-2 shows the limiting load-deformation relationships for the dynamic and static cases. If a certain load Rd is dynamically applied we move instantly from 0 to C. On the contrary, if load is applied "statically," the model deforms slowly and we move along path OA. If Eq. (6-3) is used to plot the curves OAB and OCD, the comparison with actual data is shown in Fig. 6-5.* It is seen that the lines for the ultimate values of dynamic and static condition are practically identical.

*Detailed calculations, see Appendix E.

Chapter VII

CONCLUSIONS

Since the research effort is still under way, any conclusions must, of necessity, be tentative. With this in mind, the main conclusions from the work reported herein may be summarized as follows.

Nature of Load-Deformation Relation for Cohesionless Soil. These tests have clearly indicated that the load-deformation curve for cohesionless soils shows significant non-linearities. Thus, at best, it is necessary to use modulus values which are functions of the load or deformation level, or to use modulus values which are approximately constant through some range of load or deformation.

Loading-Rate Effects. Although the principal purpose of the research was to investigate the characteristics of dynamic load-deformation relationship for saturated cohesionless soil, the test results have demonstrated that the deformation-rate effects can be separated into two basic sources:

1. Increased grain-to-grain resistance as observed in dry specimens,

2. Changes in pore-water pressure owing to the dilitation characteristics of cohesionless soil.

Loading-Rate Effect Upon Compressive Strength. An increase of from 50% to 80% in the compressive

strength can be expected in undrained saturated triaxial tests on dense Ottawa sand specimens, and 5% to 20% for saturated medium dense Ottawa sand in going from the static to high rate of 120 in. per sec. An increase of up to 40% in the compressive strength was also observed in undrained saturated triaxial compressive tests on Victoria fine sand from the static rate to high rate of loading (120 in. per sec.).

Damping Properties of Saturated Ottawa Sand. In order to obtain an analytical solution for the pile-soil system, it is necessary to assume some model for the material. Therefore, the response of the system can be interpreted in terms of material constants. It is realized that the behavior of cohesionless soil is so complicated that no simple model will completely describe such complex material. However, the Kelvin body was selected as a compromise between the conflicting requirements of realism and simplicity. The results of the dynamic and the static tests with the same testing conditions (initial void ratio and lateral confining pressure) indicate that in order to use this model, the damping factor varies with the rate of deformation. Values of damping factor for use in wave equation analysis based on present knowledge, are presented in Table 6-1.

Mechanical Equation of State. Finally, it should be emphasized that the present state of knowledge of dynamic behavior of soils is still only embryonic. Considerable progress has been made, of course, in the definite establishment of certain phenomenological features, e.g., all cohesionless soil will exhibit a greater strength under dynamic than under static condtions. However, the limited available data has thus far prevented the construction of rational relations involving load-deformation-time derivatives which would be useful for the evaluation of dynamic problems in soil mechanics. Further work is needed before any form of a mechanical equation of state can be established with any degree of certainty and accuracy.

Chapter VIII

RECOMMENDATIONS

The research reported herein has shown the pore-water pressure to be of primary importance in influencing the dynamic load-deformation characteristics of cohesionless soils. Further studies have been indicated as questions developed during this research. The following are a few areas where further research would be of benefit to engineers in understanding the soil-water system subjected to dynamic loading.

The effect of pore-water pressure distribution during a dynamic test would be necessary to give a broader and fundamental understanding of the characteristics of pore-water pressure.

An extension of the study reported herein to determine the dynamic load-deformation characteristics on very loose cohesionless soils would lead to a more complete understanding of nature of dilation in sand.

Results of the tests presented in Fig. 5-13 have made it apparent that the initial conditions of the specimen must be emphasized. A program of initial condition study should be undertaken. This program should begin with the study of a well graded sand and a common clay, and then proceed to more complex types of soil.

In view of the understanding and applicability of tests results of soils, it is felt that the best approach lies in a comprehensive study of the behavior of pore-water pressure under dynamic load conditions. Therefore, a new load cell permitting drainage should be undertaken.

Furthermore, study of the structural behavior of the various types of load cell under dynamic loading conditions is warranted.

Finally, an extension of the study of the dynamic effect on cohesive soil is of value to the application of the wave equation in pile driving.

References

1. Bishop, A. W. and Eldin, G., "Undrained Triaxial Tests on Saturated Sands and Their Significance in the General Theory of Shear Strength," Géotechnique, Vol. II, London, 1950.
2. Bishop, A. W. and Henkel, D. J., *The Measurement of Soil Properties in the Triaxial Test*, 2nd Edition, Edward Arnold (Publishers) Ltd., London, 1962.
3. Buchanan, S. J., "Soil Mechanics—Lecture Notes," (unpublished), Texas A&M University, College Station, Texas, 1963.
4. Casagrande, A., and Shannon, W. L., "Research on Stress Deformation and Strength Characteristics of Soils and Soft Rock Under Transient Loading," Soil Mechanics Series No. 31, Harvard University, Cambridge, Massachusetts, 1948.
5. Chan, P. C. and Hirsch, T. J., "An Annotated Bibliography—Soil Dynamics and Soil Rheology," Report of the Texas Transportation Institute, Texas A&M University, 1960.
6. Chen, L. S., "An Investigation of Stress-Strain Characteristics of Cohesionless Soils by Triaxial Compression Tests," Proceedings, 2nd International Conference on Soil Mechanics, Vol. V, Rotterdam, 1948.
7. Coulomb, C. A., "Essai sur une Application des regles de Maximis et Minimis a Quelques Problemes de Statique, Relatifs a l' Architecture," Mem. Acad. Roy. Pres. Div. Sav., Vol. 7, Paris, 1776.
8. Cummings, A. E., "Dynamic Pile Driving Formulas," *Contributions to Soil Mechanics*, Boston Society of Civil Engineers, Boston, Massachusetts, 1925-1940.
9. Deresiewicz, H., "Mechanics of Granular Matter," Advances in Applied Mechanics, Vol. 5, pp. 233-306, John Wiley, New York, New York, 1956.
10. Gibson, R. E., "Experimental Determination of the True Cohesion and True Angle of Internal Friction in Clay," Proceedings, 3rd International Conference of Soil Mechanics and Foundation Engineering, Vol. I, Zurich, Switzerland, 1953.
11. Glanville, W. H., Grime, G., and Davies, W. W., "The Behavior of Reinforced Concrete Piles During Driving," Journal of the Institute of Civil Engineers, 1935.
12. Glanville, W. H., Grime, G., Fox, E. N., and Davies, W. W., "An Investigation of the Stresses in Reinforced Concrete Piles During Driving," British Building Research Board Technical Paper No. 20, Dept. of Scientific and Industrial Research, His Majesty's Stationery Office, London, 1938.
13. Hirsch, T. J., "Stress in Long Prestressed Concrete Pile During Driving," Report of the Texas Transportation Institute, A&M College, 1962.
14. Hirsch, T. J., "Computer Study of Variables Which Affect the Behavior of Concrete Piles During Driving," Report of the Texas Transportation Institute, Texas A&M University, 1963.
15. Hirsch, T. J., "A Report on Field Tests of Prestressed Concrete Piles During Driving," Report of the Texas Transportation Institute, Texas A&M University, 1963.
16. Hirsch, T. J., "Fundamental Design and Driving Considerations for Concrete Piles," paper presented to the 45th annual meeting of the Highway Research Board, Washington, D. C., 1966.
17. Hvorslev, J. M., "Ueber die Festigkeitseigenschaften gestörter bindiger Böden," Danmarks Naturvidenskabelige Samfund, Ingeniörviden-skabelige Skrifter, Series A. No. 45, Copenhagen.
18. Isaacs, D. V., "Reinforced Concrete Pile Formulae," Transactions, Institute of Engineers, Australia, Vol. 12, 1931.
19. Klausner, Y., "The Mechanical Behavior of Soils," Princeton University, New Jersey, 1960.
20. Reiner, M., "Rheology," *Handbuch der Physik*, Vol. 6, Edited by S. Flügge, Springer Verlag, Berlin, Germany, pp. 435-550, 1958.
21. Reynolds, O., "On the Dilatancy of Media Composed of Rigid Particles in Contact, with Experimental Illustrations," Philosophical Magazine, Series 5, Vol. 20, London, 1885.
22. Rowe, P. W., "The Stress-Dilatancy Relation for Static Equilibrium of an Assembly of Particles in Contact," Proceedings of Royal Society (London), Series A, Vol. 269, pp. 500-527, 1962.
23. Samson, C. H. Jr., "Pile-Driving Analysis by the Wave Equation (Computer Application)," Report of the Texas Transportation Institute, A&M College of Texas, 1962.
24. Samson, C. H. Jr., Hirsch, T. J., and Lowery, L. L., "Computer Study of Dynamic Behavior of Piling," a paper presented to 3rd Conference on Electronic Computation, ASCE, Boulder, Colorado, 1963.
25. Seed, H. B. and Lungren, R., "Investigation of the Effect of Transient Loading on the Strength and Deformation Characteristics of Saturated Sands," Proc. ASTM, Vol. 54, 1954.
26. Skempton, A. W., "The Pore-Pressure Coefficients A and B," Géotechnique, Vol. IV, London, 1954.
27. Smith, E. A. L., "Impact and Longitudinal Wave Transmission," Trans. ASME, 1955.
28. Smith, E. A. L., "Pile-Driving Analysis by the Wave Equation," Trans. ASCE, Vol. 127, Part 1, 1962.
29. Steinman, D. B. and Watson, S. R., "Bridges and Their Builders," Dover Publications Inc., New York, New York, pp. 26-84.
30. Taylor, D. W., *Fundamental Soil Mechanics*, John Wiley and Sons, Inc., New York, New York, (see Chapter 11), 1948.
31. Terzaghi, K., "The Rigidity of Plastic Clays," Journal of Rheology, Vol. 2, pp. 253-262, 1931.

32. Terzaghi, K., *Theoretical Soil Mechanics*, John Wiley and Sons, Inc. New York, New York, (see Chapters 16, 17, 18, and 19), 1948.

33. Terzaghi, K., and Peck, R., *Soil Mechanics in Engineering Practice*, John Wiley and Sons, Inc., New York, New York, (see Chapter 2), 1948.

34. Todhunter, I. and Pearson, K., *A History of the Theory of Elasticity and Strength of Materials*, Dover Publications, Inc., New York, New York, Vol. 2, p. 669, 1960.

35. Truesdell, C., "The Mechanical Foundations of Elasticity and Fluid Dynamics," Journal of Mathematics and Mechanics, Department of Mathematics, Indiana University, Indiana, Vol. 1, pp. 125-297, 1952.

36. Whitman, R. W., "The Behavior of Soils Under Transient Loadings," Proceedings, 4th International Conference on Soil Mechanics, Vol. I, London, 1957.

37. Whitman, R. V., "Physics of Granular Systems — Lecture Notes," (unpublished), Massachusetts Institute of Technology, Cambridge, Massachusetts, 1963.

38. Whitman, R. V., and Healey, K. A., "Shear Strength of Sands During Rapid Loadings," Journal of the Mechanics and Foundation Division, ASCE, April, 1962.

Appendix A

SUMMARY OF TEST RESULTS

1. Ottawa Sand—Saturated State

Table A-1 — Test No. OSU-1
σ_3=45.0 psi; e_0=0.50; h=18.0 in.*

Load (lb.)	Deformation (in.)
593	0.000
800	0.010
928	0.010
1100	0.020
1235	0.038
1310	0.082
1358	0.255
1352	0.410
1328	0.525
1293	0.620
1200	0.650

*σ_3 = lateral confining pressure
e_0 = initial void ratio
h = height of weight fall

Table A-2 — Test No. OSU-2
σ_3=30.0 psi; e_0=0.50; h=18.0 in.

Load (lb.)	Deformation (in.)
543	0.000
678	0.008
842	0.010
937	0.023
1048	0.062
1117	0.120
1148	0.165
1172	0.260
1143	0.365
1100	0.450
1070	0.540
1065	0.607
1066	0.656

Table A-3 — Test No. OSU-3
σ_3=15.0 psi; e_0=0.50; h=18.0 in.

Load (lb.)	Deformation (in.)
179	0.000
272	0.018
359	0.038
430	0.059
530	0.083
656	0.120
723	0.142
781	0.179
838	0.262
837	0.300
810	0.430
722	0.508
752	0.591

Table A-4 — Test No. OSU-4B
σ_3=45.0 psi; e_0=0.50; h=9.0 in.

Load (lb.)	Deformation (in.)
329	0.000
508	0.013
683	0.022
809	0.033
1020	0.090
1085	0.142
1118	0.208
1103	0.300
1081	0.358

Table A-5 — Test No. OSU-4A
σ_3=45.0 psi; e_0=0.50; h=9.0 in.

Load (lb.)	Deformation (in.)
293	0.000
775	0.017
972	0.040
1093	0.100
1128	0.190
1088	0.310
1053	0.415
1060	0.480

Table A-6 — Test No. OSU-5
σ_3=30.0 psi; e_0=0.50; h=9.0 in.

Load (lb.)	Deformation (in.)
297	0.000
604	0.027
733	0.048
900	0.102
982	0.190
948	0.292
903	0.400
861	0.430
803	0.430

Table A-7 — Test No. OSU-6
σ_3=15.0 psi; e_0=0.50; h=9.0 in.

Load (lb.)	Deformation (in.)
175	0.000
307	0.050
403	0.087
500	0.118
580	0.160
653	0.218
664	0.274
662	0.371
653	0.482
648	0.553

Table A-8 — Test No. OSU-7
σ_3=45.0 psi; e_0=0.50; h=3.0 in.

Load (lb.)	Deformation (in.)
297	0.000
605	0.028
732	0.049
900	0.102
980	0.190
950	0.292
907	0.400
862	0.429
800	0.430

Table A-9 — Test No. OSU-8
σ_3=30.0 psi; e_0=0.50; h=3.0 in.

Load (lb.)	Deformation (in.)
108	0.000
275	0.028
408	0.050
517	0.065
680	0.080
832	0.160
838	0.310
796	0.408
770	0.480

Table A-10 — Test No. OSU-9
σ_3=15.0; e_0=0.50; h=3.0 in.

Load (lb.)	Deformation (in.)
95	0.000
250	0.070
350	0.110
440	0.155
465	0.213
470	0.275
470	0.373
465	0.505
460	0.585
450	0.700

Table A-11 — Test No. OSR-1
σ_3=45.0; e_0=0.50; Static

Load (lb.)	Deformation (in.)
0	0.000
75	0.012
212	0.017
421	0.020
552	0.030
620	0.060
685	0.160
703	0.220
715	0.363
728	0.460
720	0.580
662	0.740

Table A-12 — Test No. OSR-2
σ_3=30.0 psi; e_0=0.50; Static

Load (lb.)	Deformation (in.)
0	0.000
80	0.018
167	0.029
300	0.042
407	0.050
483	0.060
578	0.145
620	0.282
634	0.412
638	0.510
636	0.602
633	0.718

Table A-13 — Test No. OSR-3
σ_3=15.0 psi; e_0=0.50; Static

Load (lb.)	Deformation (in.)
0	0.000
73	0.023
173	0.038
235	0.042
312	0.060
406	0.112
442	0.140
460	0.213
472	0.310
475	0.408
463	0.507
460	0.700

Table A-14 — Test No. OSU-10
σ_3=45.0 psi; e_0=0.60; h=18.0 in.

Load (lb.)	Deformation (in.)
295	0.000
460	0.023
597	0.041
670	0.060
698	0.072
733	0.100
760	0.200
722	0.325
676	0.440
660	0.612

Table A-15 — Test No. OSU-11
σ_3=30.0 psi; e_0=0.60; h=18.0 in.

Load (lb.)	Deformation (in.)
90	0.000
198	0.013
270	0.020
371	0.043
412	0.050
474	0.113
503	0.180
518	0.253
507	0.330
483	0.403
434	0.554
417	0.663

Table A-16 — Test OSU-12
σ_3=15.0 psi; e_0=0.60; h=18.0 in.

Load (lb.)	Deformation (in.)
87	0.000
175	0.028
283	0.049
342	0.072
396	0.133
425	0.240
401	0.348
398	0.404
398	0.452

Table A-17 — Test OSU-13
σ_3=45.0 psi; e_0=0.60; h=9.0 in.

Load (lb.)	Deformation (in.)
158	0.000
300	0.028
440	0.049
538	0.062
660	0.112
771	0.178
748	0.252
677	0.305
662	0.400
659	0.473
670	0.602

Table A-18 Test No. OSU-14
σ_3=30.0 psi; e_0=0.60; h=9.0 in.

Load (lb.)	Deformation (in.)
252	0.000
362	0.022
412	0.042
453	0.083
475	0.175
479	0.240
443	0.377
418	0.477
407	0.538
400	0.703

Table A-19 Test OSU-15
σ_3=15.0 psi; e_0=0.60; h=9.0 in.

Load (lb.)	Deformation (in.)
80	0.000
145	0.021
208	0.043
304	0.092
350	0.140
388	0.220
386	0.292
367	0.397
328	0.502

Table A-20 Test No. OSU-16
σ_3=45.0 psi; e_0=0.60; h=3 in.

Load (lb.)	Deformation (in.)
238	0.000
414	0.048
502	0.087
565	0.108
638	0.197
637	0.285
628	0.413
565	0.457
475	0.472

Table A-21 Test No. OSU-17
σ_3=30.0 psi; e_0=0.60; h=3.0 in.

Load (lb.)	Deformation (in.)
85	0.000
190	0.028
295	0.058
355	0.103
4.43	0.215
448	0.317
445	0.430
350	0.520

Table A-22 Test No. OSU-18
σ_3=15.0 psi; e_0=0.60; h=3.0 in.

Load (lb.)	Deformation (in.)
45	0.000
137	0.033
257	0.062
324	0.095
358	0.190
370	0.318
378	0.441
330	0.570

Table A-23 Test No. OSR-4
σ_3=45.0 psi; e_0=0.60; Static

Load (lb.)	Deformation (in.)
0	0.000
65	0.020
173	0.041
335	0.065
434	0.078
515	0.114
560	0.164
607	0.263
610	0.418
595	0.567
592	0.643
590	0.780

Table A-24 Test No. OSR-5
σ_3=30.0 psi; e_0=0.60; Static

Load (lb.)	Deformation (in.)
0	0.000
100	0.027
233	0.048
300	0.073
354	0.106
390	0.155
408	0.214
410	0.300
417	0.370
428	0.430
420	0.509
417	0.585
415	0.635

Table A-25 Test No. OSR-6
σ_3=15.0 psi; e_0=0.60; Static

Load (lb.)	Deformation (in.)
0	0.000
115	0.027
208	0.040
322	0.095
347	0.182
354	0.300
357	0.403
354	0.562
350	0.660
340	0.810

2. Ottawa Sand—Dry State

Table A-26 Test No. ODR-2
σ_3=30.0 psi; e_0=0.50; h=9.0 in.

Load (lb.)	Deformation (in.)
115	0.000
323	0.034
472	0.067
573	0.130
612	0.225
608	0.300
568	0.443

Table A-27 Test No. ODR-5
σ_3=30.0 psi; e_0=0.60; h=9.0 in.

Load (lb.)	Deformation (in.)
40	0.000
198	0.072
307	0.133
352	0.200
334	0.326
281	0.370

Table A-28 — Test No. ODR-7; σ_3=30.0 psi; e_0=0.50; h=3.0 in.

Load (lb.)	Deformation (in.)
113	0.000
223	0.027
447	0.103
516	0.160
570	0.270
526	0.462

Table A-29 — Test No. ODR-8; σ_3=30.0 psi; e_0=0.60; h=3.0 in.

Load (lb.)	Deformation (in.)
37	0.000
198	0.067
311	0.133
336	0.227
318	0.370
314	0.441

Test A-30 — Test No. ODR-9; σ_3=30.0 psi; e_0=0.50; h=18.0 in.

Load (lb.)	Deformation (in.)
231	0.000
340	0.019
478	0.042
600	0.110
668	0.201
675	0.300
653	0.382
617	0.540

Table A-31 — Test No. ODR-10; σ_3=30.0 psi; e_0=0.60; h=18.0 in.

Load (lb.)	Deformation (in.)
57	0.000
203	0.054
292	0.090
388	0.218
372	0.310
346	0.430

Table A-32 — Test No. ODR-11; σ_3=30.0 psi; e_0=0.50; Static

Load (lb.)	Deformation (in.)
0	0.000
201	0.046
362	0.065
447	0.110
520	0.156
547	0.235
540	0.481
537	0.610
530	0.725

Table A-33 — Test No. ODR-12; σ_3=30.0 psi; e_0=0.60; Static

Load (lb.)	Deformation (in.)
0	0.000
73	0.026
196	0.074
271	0.128
326	0.267
336	0.337
315	0.510
328	0.710

3. Victoria Sand, Victoria, Texas—Saturated State

Table A-34 — Test No. VSU-1; σ_3=15.0 psi; e_0=0.53; h=18.0 in.

Load (lb.)	Deformation (in.)
278	0.000
436	0.018
667	0.033
812	0.052
900	0.090
952	0.132
987	0.223
925	0.402
883	0.518

Table A-35 — Test No. VSU-2; σ_3=15.0 psi; e_0=0.53; h=9.0 in.

Load (lb.)	Deformation (in.)
177	0.000
502	0.036
728	0.107
829	0.182
786	0.264
767	0.361
752	0.440

Table A-36 — Test No. VSU-3; σ_3=15.0 psi; e_0=0.53; h=3.0 in.

Load (lb.)	Deformation (in.)
162	0.000
364	0.032
575	0.126
720	0.186
716	0.274
651	0.372
610	0.460

Table A-37 — Test No. VSU-4; σ_3=15.0 psi; e_0=0.53; Static

Load (lb.)	Deformation (in.)
0	0.000
116	0.028
327	0.061
426	0.078
547	0.113
683	0.218
637	0.300
638	0.418
638	0.540
638	0.700
634	0.823

TABLE A-38. COEFFICIENT OF SPRING CONSTANT (K')

Test No.	Initial Void Ratio	Lateral Confining Pressure (psi)	Coefficient Spring Constant (lb. per in.)
OSR-1	0.50	45.0	10,000.0
OSR-2	0.50	30.0	8,800.0
OSR-3	0.50	15.0	6,800.0
OSR-4	0.60	45.0	6,000.0
OSR-5	0.60	30.0	5,500.0
OSR-6	0.60	15.0	5,240.0
ODR-11	0.50	30.0	4,780.0
ODR-12	0.60	30.0	3,800.0
VSR-4	0.53	15.0	7,430.0

Appendix B

DERIVATION OF EQS. (2-13) & (2-14)

The array under consideration is shown in Fig. B-1 (c.f. Fig. 2-5). This array is of two dimension, being only a unit dimension in depth. The stresses applied to the array, σ_1, and σ_3, have the same meaning as it was mentioned previously in triaxial compression tests. The forces shown in Fig. B-1, F_1, and F_3 are the vertical and horizontal components of the forces at the contact points. From the geometry of the packing, assuming $F_o = 0$, it can be shown that

$$2F_1 = 2R(\sigma_1)$$

or

$$F_1 = R(\sigma_1) \tag{B-1}$$

also

$$2F_3 = 2\sqrt{3}\,R(\sigma_3)$$

or

$$F_3 = \sqrt{3}\,R(\sigma_3) \tag{B-2}$$

Now the normal and tangetial components of F_1, and F_3, N and T, can be readily shown, respectively:

$$N = \frac{\sqrt{3}}{2}F_1 + \frac{1}{2}F_3$$

$$= \frac{\sqrt{3}}{2}R(\sigma_1 + \sigma_3) \tag{B-3}$$

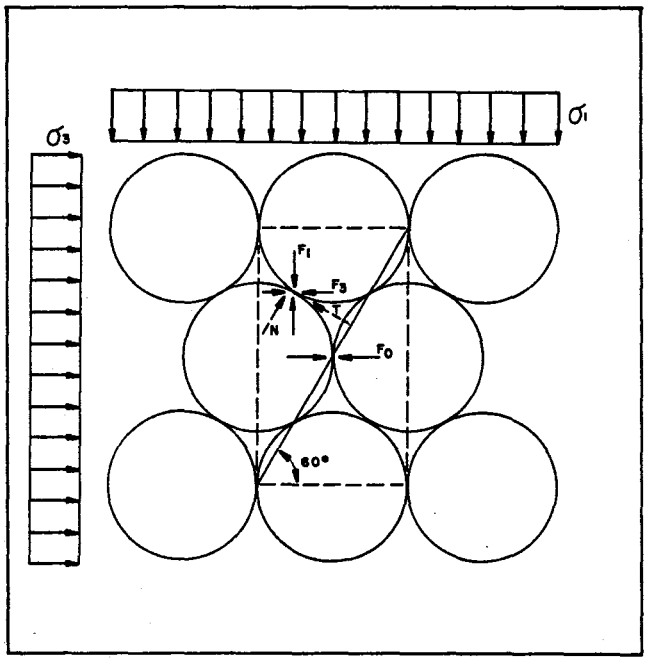

Figure B-1. Dense packing (after Whitman, Ref. 33).

$$T = \frac{1}{2}F_1 - \frac{\sqrt{3}}{2}F_3$$

$$= \frac{R}{2}(\sigma_1 - 3\sigma_3) \tag{B-4}$$

Appendix C

DERIVATION OF EQ. (4-2)

In order to examine the pore-water pressure set up in an undrained compressure test, it is necessary to consider the relationship of volume change between the pore-water and soil skeleton.

Let C_s denote the compressibility of the soil skeleton.

C_u the compressibility of the pore-water

V the initial volume of sample

n the initial porosity

$\delta\bar{\sigma}$ change in effective stress

δ_u change in pore-water pressure

It then follows that the volume changes can be written:

(a) decrease in volume of the soil skelton $= C_s V \cdot \delta\bar{\sigma}$

(b) decrease in volume of pore-water $= C_u \cdot n \cdot V \cdot \delta_u$

Since the drainage of the sample was prevented, the decreases in volume of the soil skeleton and pore-water must be equal, that is to say:

$$C_s \cdot V \cdot \delta\bar{\sigma} = C_u \cdot nV \cdot \delta u$$

or

$$C_s \cdot \delta\bar{\sigma} = C_u \cdot n \cdot \delta u \tag{C-1}$$

Now, by definition:

$$\bar{\sigma} = \sigma - u \tag{C-2}$$

Therefore Eq. (C-1) can be rewritten

$$n\,\frac{C_u}{C_s} \cdot \delta u = \delta\sigma - \delta u \tag{C-3}$$

and thus

$$\delta u = \frac{1}{1 + n\,\frac{C_u}{C_s}} \cdot \delta\sigma \tag{C-4}$$

If the pore-water and the soil skeleton are taken to be incompressible, then by definitions $\frac{C_u}{C_s} = 0$. Hence, Eq. (C-4) can be rewritten as follows:

$$\delta u = \delta\sigma \tag{C-5}$$

Appendix D

DERIVATION OF EQ. (6-1)

The rheological soil model is subjected to a stress σ_o, which will cause the model to deform in the direction indicated by X of Fig. 6-1, and stress will thereby be introduced into both branches of the model. The entire stress σ_o will be equal to the sum of the stresses in each branch and can be expressed as

$$\sigma_o = \sigma_1 + \sigma_2 \qquad \text{(D-1)}$$

In the branch containing the spring only, the stress is

$$\sigma_1 = \mu\epsilon \qquad \text{(D-2)}$$

In the branch containing the dashpot, the stress is

$$\sigma_2 = \eta \frac{d\epsilon}{dt} \qquad \text{(D-3)}$$

Therefore, substituting into Eq. (D-1) gives

$$\sigma_o = \mu\epsilon + \eta \frac{d\epsilon}{dt} \qquad \text{(D-4)}$$

Appendix E

ILLUSTRATIVE EXAMPLE—EVALUATION OF THE ULTIMATE DYNAMIC STRENGTH

Reference Fig. 6-5 and Fig. 5-6 (Tests OSR-2 and OSU-2) Basic data:

K' = spring constant $= \frac{638}{.08} = 7975$ lb. per in. (see Fig. 5-6)

J = rheological damping coef. = 0.08 (from Table 6-1, Test OSU-2)

$\dot{x}$ = rate of loading = 126 in. per sec. (10.5 ft. per sec.)

x = 0.08 in. (see Fig. 5-6)

The ultimate static strength is:

$$Rs = K'x = (7975)\ (0.08) = 638.0 \text{ lb.}$$

Then, the ultimate dynamic strength is

$$Rd = K'x\ (1 + J\dot{x}) = (638)\ (1 + 0.08 \times 10.5) = 1172 \text{ lb. (see Table A-2)}$$